The Saint-Jude landslide of May 10th, 2010, Quebec, Canada: Investigation and characterisation of the landslide and its failure mechanism

Ariane LOCAT ing. Ph.D. – Auteure principale

Département de génie civil et de génie des eaux, Université Laval
Pavillon Adrien-Pouliot, 1065 av. de la Médecine
Québec, Qc, Canada G1V 0A6
Tel : 1 418 656 2992
ariane.locat@gci.ulaval.ca

Pascal LOCAT ing. M.Sc.

Section des Mouvements de Terrain, Service de la géotechnique et de la géologie
Ministère des Transports, de la Mobilité durable et de l'électrification des transports
880 Ch. Sainte-Foy, 3ème étage
Québec, Qc, Canada G1S 2L2
Pascal.Locat@transports.gouv.qc.ca

Denis DEMERS ing. Ph.D.

Section des Mouvements de Terrain, Service de la géotechnique et de la géologie
Ministère des Transports, de la Mobilité durable et de l'électrification des transports
880 Ch. Sainte-Foy, 3ème étage
Québec, Qc, Canada G1S 2L2
Denis.Demers@transports.gouv.qc.ca

Serge LEROUEIL Ph.D.

Département de génie civil et de génie des eaux, Université Laval
Pavillon Adrien-Pouliot, 1065 av. de la Médecine
Québec, Qc, Canada G1V 0A6
serge.leroueil.@gci.ulaval.ca

Denis ROBITAILLE ing.

Section des Mouvements de Terrain, Service de la géotechnique et de la géologie
Ministère des Transports, de la Mobilité durable et de l'électrification des transports
880 Ch. Sainte-Foy, 3ème étage
Québec, Qc, Canada G1S 2L2
Denis.Robitaille@transports.gouv.qc.ca

Guy LEFEBVRE Ph.D.

Département de génie civil, Université de Sherbrooke
2500, boul. de l'Université, Sherbrooke
Québec, Qc, Canada J1K 2R1
Guy.Lefebvre@USherbrooke.ca

Abstract

A landslide occurred on May 10, 2010, along the Salvail River, in the municipality of Saint-Jude, Quebec. Debris of the landslide was formed of blocks clay having horst and graben shapes, typical of spreads in sensitive clays. A detailed investigation was carried out by the Ministère des Transports, de la Mobilité durable et de l'électrification des transports du Québec in collaboration with Université Laval, with the objective of characterizing this landslide, determining the causes and learning about its failure mechanism. The soil involved is a firm, grey, sensitive lightly overconsolidated clay with some silt. Data from piezometers installed near the landslide indicated artesian conditions underneath the Salvail River. Cone penetration tests allowed to location of two failure surface levels. The first one starting 2.5 m below the initial river bed and extending horizontally up to 125 m and a second one 10 m higher reaching the backscarp. Investigation of the debris with onsite measurements, light detector and ranging surveys, cone penetration tests, and boreholes allowed a detailed geotechnical and morphological analysis of the debris and reconstitution of the dislocation mechanism of this complex spread.

Key words: landslide, spread, sensitive clay, geotechnical investigation, horst, graben.

Résumé

Un glissement est survenu le 10 mai 2010 le long de la rivière Salvail, dans la municipalité de Saint-Jude au Québec. Les débris de ce glissement étaient formés de blocs d'argile ayant la forme d'horst et de grabens, typique des étalements dans les argiles sensibles. Le Ministère des Transports, de la Mobilité durable et de l'électrification des transports du Québec et l'Université Laval ont réalisé l'investigation détaillée de ce glissement de terrain, dans le but de le caractériser, d'en déterminer les causes et d'en apprendre d'avantage sur le mécanisme de rupture. Le sol impliqué est une argile sensible grise avec un peu de silt, de consistance ferme, légèrement surconsolidée. Les piézomètres installés à proximité du glissement indiquent des conditions artésiennes sous la rivière Salvail. L'utilisation du piézocône a permis de localisée deux niveaux de surfaces de ruptures. L'un a 2.5 m sous la position initiale de la rivière, s'entendant horizontalement sur 125 m, et l'autre 10 m plus haut, allant jusqu'à l'escarpement arrière. L'investigation des débris par mesures prises sur le terrain, levées de télédétection par laser, piézocônes et forages a permis une analyse géotechnique et morphologique détaillée de ces derniers et la reconstitution du mécanisme de dislocation de ce glissement complexe.

Mots-clés: glissement de terrain, étalement, argile sensible, investigation géotechnique, horst, graben.

Introduction

On the 10th of May 2010, at 08:25 pm, a large landslide occurred in the municipality of Saint-Jude, Québec, about 50 km north-east of Montréal (Figure 1). Four people were killed as their house was destroyed by the movement and one man was injured falling with his truck in the crater of the landslide while driving on the North Salvail road. The landslide occurred in a sensitive Champlain Sea clay deposit along the Salvail River. The original slope had a height of about 22 m and an inclination varying between 12 and 20°. A section of about 275 m long, parallel to the river, was affected by the landslide. The retrogression of the landslide, from the initial crest of the slope to the backscarp of the landslide, was 80 m. The total volume of debris was about 520 000 m^3. The soil mass dislocated in blocks of more or less intact material having horst and graben shapes. These structures present in the debris of the landslide are typical of spreads (Cruden and Varnes 1996; Locat et al. 2011a; and Hungr et al. 2014). This type of landslide can be hazardous to affected people and infrastructures as it occurs suddenly, without any warning and can cover large areas.

The Ministère des Transports, de la Mobilité durable et de l'électrification des transports (MTMDET) in collaboration with Université Laval carried out a detailed investigation in order to characterise this landslide and to specify its failure mechanism. The investigation included field observations and in situ testing as well as laboratory tests that enabled the investigators to obtain information on the morphology of the landslide, the stratigraphy of the deposit and the properties of the soil involved in the landslide.

This paper begins by describing the regional context of the area where the landslide occurred. The detailed investigation performed is also presented. A discussion on the failure mechanisms, the possible aggravating and triggering factors, and the consequences of the landslide is presented followed by a conclusion to this paper.

The landslide and its regional context

The 2010 landslide involved post-glacial Champlain sea clays that were deposited between approximately 12 000 and 10 000 years ago (Ochietti 1989). In the region of Saint-Jude, the sediments filled a shallow preglacial valley, located below the modern Salvail River and extending up about 15 km in the north-east direction, below the Yamaska River (Rissmann et al. 1985). Near the landslide, sediment deposits reach a thickness up to 45 m tapering to only a 20 to 25 m thickness on both sides of this preglacial valley (Rissmann et al. 1985).

Figure 2 presents a Digital Elevation Model (DEM) of the region where the 2010 landslide occurred. The data were obtained from aerial Light Detection and Ranging (LIDAR) surveys performed after the landslide. The figure shows location of the 2010 landslide and other large retrogressive landslides that previously occurred along the Salvail River and its tributaries. 16 similar landslides can be identified in the area of the 2010 landslide.

Analysis of aerial photographs, dating back as far as 1931, indicated that seven large landslides (> 1 ha) occurred along the Salvail River between the Yamaska River and the municipality of Saint-Jude, between 1931 and present, while the rest of the landslides inferred from LIDAR occurred prior 1931, at unknown dates. When observing these aerial photographs and LIDAR data of the site of the 2010 event, it was observed that the south part of the 2010 event involved debris of a landslide that occurred at an unknown date. In addition, observation of aerial photographs of the site since 1950 indicated that two slides recently occurred (present on the 2009 aerial photographs). These two slides had a width of 75 m and 20 m respectively. It points out that erosion may have been active near the foot of the slope. The debris of these slides were gradually eroded by the river and vanished with time.

Figure 3 presents an aerial photograph taken on May 11th 2010, the day after the landslide. It can be seen that the debris completely blocked the Salvail River, creating flooding upstream and leaving downstream completely dry. Observations on site showed that ridges created by horsts and grabens covered with grass, trees and pieces of road were forming the debris. Figure 4 presents a general view of the south part of the landslide showing this complex debris. Horsts are blocks that form triangular ridges of relatively intact material in the debris and have sharp tips pointing upward. Grabens are blocks having flat tops generally covered with grass and trees. These structures show a “thumbprint microrelief pattern” when viewed on aerial photographs. Figures 5 and 6 present a closer look of such blocks, showing horsts, with horizontal stratifications, and grabens covered by pieces of road or grass. Note the electric pole still standing on the right of the photograph on Figure 5 and trees standing in the debris after the landslide on Figure 6. Horsts and grabens are typical of spreads (Cruden and Varnes 1996; Hungr et al. 2014) occurring in sensitive clays and were described by Odenstad (1951), Carson (1979a, b), Tavenas (1984), Grondin and Demers (1996), Demers et al. (2000), Locat et al. (2008), and Locat et al. (2011a). In addition to horsts and grabens, inclined slices were observed in the debris. Figure 7 presents a photograph of these inclined sliced located in the south part of the landslide.

Investigation methods

Investigation of the site started the day after the event, on May 11th 2010, and included detailed field observations, analysis of aerial photographs and LIDAR surveys. The investigation also included 4 boreholes, 35 piezocone tests with pore water pressure measurement (CPTU), 2 field vane shear test profiles, 3 piezometer nests and 4 trenches located on Figure 3.

Aerial photographs of the site were taken on May 11th 2010, a few hours after the event while excavation works were ongoing near the house (Figure 3). Comparing these aerial photographs to previous ones allowed the identification several targets and the measurement of their displacement due to ground movement. This gives valuable information on the kinematic of failure.

Detailed topographic data of the area where the 2010 landslide occurred was obtained from LIDAR surveys. Two types of surveys were performed: aerial LIDAR survey, performed on May 13th 2010, and terrestrial LIDAR survey taken on May 19th and 20th 2010. The first survey covered the entire landslide and its surroundings. The second one covered only the south-east part of the debris, near the backscarp of the landslide (about zone 4 on Figure 3).

The intact soil, outside the 2010 landslide, was characterized by 9 CPTUs, 2 boreholes and 2 field vane shear test profiles near the borehole locations. The locations of 6 of these CPTUs are shown on Figure 3. One of them, at location 32060, was done by the MTMDET in 2004, six years before the landslide. It is now located inside the landslide and gives information on soil conditions before the event. These CPTUs give detailed and continuous strength profiles (corrected tip resistance, q_t, water pressure, u_{base}, and sleeve friction resistance), and thus give information on the stratigraphy of the deposit. This information, combined with samplings from the boreholes and shear strength profiles from the field vane shear tests ($S_{u\ vane}$), enables the determination of the geotechnical properties of the material involved in the landslide. It is worth noting that no feature such as a weak layer or a softened zone was observed on the 2004 CPTU that could explain the 2010 landslide (see section Location of the failure surface and figure 14).

The debris were studied with 26 CPTUs and 2 boreholes (32140 and 32141). Their locations are shown on Figure 3. These CPTUs enabled the precise location of the failure surface and to observe the stratigraphy and the characteristics of the disturbed debris and the soil below.

Four trenches were dug in the debris to observe the stratigraphy of intriguing morphological structures and to get a better understanding of the dislocation mechanism of the soil mass. Their locations are shown on Figure 3 by white rectangles with their longer side oriented parallel to the trench.

Pneumatic and Casagrande types piezometers were installed at different locations south of the landslide. Piezometers nests were installed at location 32146, on the plateau far behind the top of the slope, at location 32100, near the crest of the slope, as well as at location 32145, near the base of the slope.

Samples of soft clayey materials near the landslide and in the debris were taken with thin wall tubes ~70 mm in diameter obtained using a piston sampler. In stiff and coarse materials, a split-spoon sampler was used. Several of the thin wall tubes were examined with computerized axial tomography scans (CAT scan) to obtain images of the stratigraphy of the samples.

The geotechnical properties of the soil specimens were studied in the laboratory with the following tests: particle size distribution, water content (w), consistency limits, pore water salinity estimated by electric resistivity, intact ($S_{u\ cone}$) and remoulded (S_{ur}) shear strengths with the Swedish fall cone, oedometer tests and falling-head hydraulic permeability tests. In addition, the shear behaviour of the soil involved in the landslide was studied with triaxial compression tests in undrained conditions (CIU) and constant volume (undrained) direct simple shear tests (DSS) on intact specimens.

Geotechnical characterization of intact soil

Morphology of the slope before failure

Cross-sections of the slope before and after the landslide are presented on Figures 8 and 9 (see Figure 3 for location). The topography before failure is from the DEM built from aerial photographs taken in 2004. The plateau at the top of the natural slope is at an elevation of about 28 m above sea level and the Salvail River bed is located at an elevation of about 6 m. The total height of the slope at the site of the landslide was 22 m. The angle of the slope before failure ranged from 12° to 16° for the upper 12 m and was about 20° for the lower 10 m.

Stratigraphy and geotechnical properties of the intact soil

Investigations carried out in intact material at locations 32092 and 32100 (boreholes, CPTUs, field vane shear tests and piezometers, located on Figure 3), made it possible to obtain information on the stratigraphy and geotechnical properties of the intact soil outside the footprint of the landslide. The 2 boreholes and 9 CPTUs carried out in the intact deposit show the remarkable uniformity of the soil properties. The results from the CPTUs done in 2010 were also comparable to results from the CPTU carried out in 2004 at location 32060 inside the footprint of the landslide. Borehole at location 32100 gave similar results to the one at location 32092, located at an elevation 0.06 m lower, only the geotechnical profile obtained at location 32100 near the crest of the slope, south of the landslide (white star on Figure 3), is presented in this paper (Figure 10). Five distinct units can be identified in the intact soil overlying the bedrock. The bedrock was sampled at location 32092, data are therefore not shown on Figure 10. Readers are referred to Locat et al. (2011b) for further details.

The top unit, unit A, is a 3.8 m thick, (from elevation 28 to 24.2 m) dense, grey brown, sandy crust. Samples from this unit were taken at location 32092 and are not presented here. Readers are referred to Locat et al. (2011b) for further details. The water content varies between 24 and 78% and the intact shear strength from CPTU ($S_{u\ CPTU}$), between 50 and 165 kPa (calculated with a dimensionless parameter for CPTU shear strength, N_{kt}, estimated to 13.5). Based on the average water content, unit weight is approximately 18.6 kN/m^3.

Unit B is a 22.2 m thick (from elevation 24.2 to 2 m), firm, grey, sensitive clay deposit very uniform with some silt. The clay is characterized by light and dark grey beds having thickness of about 5 cm, near the top of the unit, getting thinner than 2.5 cm near the bottom. Clay fraction is between 50 and 80%. The water content is about 65% over the entire unit. The plastic limit (w_P) has a mean value of 26% and is generally constant throughout the depth of the unit. The liquid limit (w_L) increases from 45 to 65% with depth. The liquidity index (I_L) thus decreases with depth from about 2.0 to 1.0, corresponding to remoulded shear strength varying respectively from 0.3 to 1.6 kPa, according to Leroueil et al. (1983) relationship. The salinity of the pore water, determined through electrical resistivity on samples taken at location 32092, varies from 1 g/L, at a depth of 8 m, to 7 g/L at a depth of 28 m. These values correlate well with the increase in liquidity limit with depth. The intact field vane shear strength increases almost linearly with depth from 25 to 65 kPa from the top to the bottom of the unit. Given the intact and remoulded shear strengths of this unit, its sensitivity varies from 80 to 40 from the top to the bottom of the unit. The preconsolidation pressure (σ'_p) increases from 120 kPa, at a depth of 8 m, to 220 kPa, at a depth of 23 m. The overconsolidation ratio ($OCR = \sigma'_p / \sigma'_v$, where σ'_v is the vertical effective stress) decreases from 1.9 to 1.2 over the same depths. The clay is therefore lightly overconsolidated. A hydraulic conductivity of 9×10^{-10} m/s was measured on a sample from a depth of 16.8 m with varying head permeability tests during an oedometer test. Unit B corresponds to a typical Champlain Sea clay deposit and was the main unit involved in the 2010 landslide.

Unit C is a 5 m thick (from elevation 2 to -3 m), stiff, silty clay of low sensitivity. Observation of samples from this unit showed that it is made of four layers. From a depth of 26.5 m to 28 m a grey silty clay with darker grey clay nodules and a few sea shells was identified. In this layer, two pinkish silty clay sub-layers (pink layer on Figure 10), having thickness of about 8 and 19 cm each and darker grey nodules, were also found at depths of 26.9 and 27.1 m. A grey silty clay layer with dark black spots has been observed from a depth of 28 m to a depth of 28.7 m (dark grey layer on Figure 10). Unit C ends with a grey silt and clay layer having thin sand and silt beds with a few sea shells. Clay fraction is around 54% through unit C. The water content decreases from 70 to 40% with depth. The plastic limit decreases from 30 to 19% and the liquid limit from 64 to 46%. The liquidity index decreases from 1 to 0.7. The shear strength throughout unit C is variable. It increases rapidly from 65 kPa to about 107 kPa between depths of 26 m to 27 m, decreases to 50 kPa at a depth of 28 m and increases again to 77 kPa at a depth of 29.5 m, to finally decrease down to 50 kPa at a depth of 31 m. This variation of shear strength defines a peak in unit C shear strength profile at a depth of 27 m.

Unit D is a 6 m thick (from elevation -3 to -9 m) very stiff, grey-brown clayey silt. Clay fraction is around 33%. The water content is around 23%. The plastic and liquid limits are 13 and 27% respectively. The liquidity index is about 0.7. The shear strength from CPTU (N_{kt} of 13.5) varies between 50 and 150 kPa. The hydraulic permeability measured with varying head permeability tests during an oedometer test is 5.5 x 10^{-10} m/s on a sample taken at a depth of 33.3 m. This unit is therefore less permeable than unit B although its grain size is coarser.Unit E is a 5 m thick (from elevation -9 to -14.6 m) deposit of hard, grey-brown, sandy silt with some clay and traces of gravel and silt. Clay fraction varies between 4 and 20%. This unit is interpreted as a till overlying the bedrock.

Unit R (lower than elevation -14.6 m) is comprised of grey sandstone and red shale bedrock.

Triaxial compression tests were performed on samples from depths of 20.5, 20.9, and 22.2 m in unit B, slightly above the river bed elevation, taken from the borehole at location 32092. Samples from depths of 20.5 and 20.9 m were isotropically consolidated in the normally consolidated range under effective stresses of 192 and 293 kPa respectively, and compressed in undrained conditions. These tests showed that the soil in unit B has a friction angle in the normally-consolidated range of 30° and a cohesion of 10 kPa. Figure 11 presents the deviatoric stress (q) and water pressure (u) vs. axial strain (ε_{1}) curves for tests performed on samples from depths of 22.2. The sample was isotropically consolidated in the overconsolidated domain at a vertical stress of 87 kPa (0.4 σ'_p) and sheared in undrained conditions (CIU_{oc}). The results indicate that the soil has a strain-softening behaviour in undrained conditions with peak shear strength of 65.6 kPa reached at an axial stain of 1.4% and a strength of 41.9 kPa reached at an axial strain of 14.6% (end of test, see Figure 11). The soil has therefore a strain-softening behaviour in undrained conditions when tested in overconsolidated conditions.

DSS tests were performed on samples from depths of 22.1 and 22.7 m in unit B at location 32092, slightly above the river elevation. Figure 12 shows the stress-strain behaviour in a shear stress (τ) vs. shear strain (γ) diagram obtained from these tests. Samples from depths of 22.1 and 22.7 m were consolidated under a vertical effective stress of 91 (0.4 σ'_p) and 170 kPa (close to in situ σ'_v at the sample depth) respectively, and sheared while keeping their height constant (constant volume) to prevent drainage and simulate an undrained conditions. The test consolidated at 91 kPa reached a peak shear strength of 47.9 kPa at a shear strain of 4.3% and at 26.8%, the shear strength had decreased to 31.9 kPa. It shows a dilatant behaviour from shear strain of 0 to 5% and then became contractant for the rest of the test. The sample consolidated at 170 kPa shows a peak shear strength of 55.6 kPa at a shear strain of 3.2% and a shear strength of 28.2 kPa at a shear strain of 31%. Both tests show strain-softening behaviours in DSS constant volume when tested at slightly to moderately overconsolidated conditions. Such large deformation shear strengths are much larger than shear strength of the remoulded soil (~1.6 kPa, near the bottom of unit B).

Ground water regime

Piezometers were installed at location 32146 on the plateau, location 32100 close to the crest of the slope, and at location 32145, near the toe of the slope (see location on Figure 3). Figure 13 presents the different piezometers installed at these locations (circles) and the measured water levels (open triangles) along cross-section D-D’ (located on Figure 3). This cross-section has been drawn perpendicular to the slope at locations 32100 and 32145. It has to be noted that piezometers at locations 32100 and 32146 are located a few meters from the cross-section D-D’ (see Figure 3). It can be observed that water levels measured at location 32146, indicate a slight downward flow with a groundwater table close to the ground surface. Similar observations are made for piezometers at location 32100 located behind the crest of the slope. On the other hand, near to the toe of the slope, at location 32145, the measured water elevations increase with the depth of piezometers. The water levels in piezometers in unit E at location 32145 are above the ground elevation (Figure

13). Therefore, upward seepage is present at the toe of the slope with high artesian water pressure conditions.

Location of the failure surface

Figures 8 and 9 show cross-sections B-B’ and C-C’ of the topography before and after the landslide (dashed and full black lines, respectively), location of the interpreted failure surface (black dots), and displacement vectors of some debris (red arrows). Locations of these cross-sections is shown on Figure 3. In this section, only cross-sections B-B’ and C-C’ are presented. Cross-section A-A’ will discussed latter in section Discussion on the landslide failure mechanism. On Figures 8 and 9, the topography after the landslide was obtained from a DEM made by combining aerial and terrestrial LIDAR surveys performed a few days after the landslide. The failure surface was defined using the difference in shear strength of the intact soil and the above remoulded debris from the 26 CPTUs performed inside the scar and located on Figure 3. An example is shown on Figure 14 where, the CPTU carried out at location 32060 in 2004, before the landslide, shows the intact strength profile of the soil and the CPTU at location 32103 shows the strength profile of the debris following landslide deformation. The difference between both profiles delimits the debris thickness having lower strength than the intact soil. The point where the strength of the soil in the debris becomes equal to the intact strength defines the elevation of the failure surface (Figure 14).

Figures 8 and 9 show that the failure surface is located at an elevation of about 3.5 m near the toe of the initial slope. This is about 2.5 m below the elevation of the Salvail River bed observed on the north of the 2010 landslide, when its course was blocked by debris. At the locations of cross-section B-B’ (Figure 8), the failure surface is horizontal over a length of about 115 m, away from the initial river location, and then rises up suddenly to an elevation of around 14 m before reaching the backscarp of the landslide. Along cross-section C-C’ (Figure 9) the failure surface is at about elevation 3.5 m for about 125 m inside the deposit and comes up to an elevation of about 14 m. Along cross-section A-A’, the main failure surface has a length of about 80 m before jumping to about an elevation of 14 m (see section Discussion on the landslide failure mechanism).

Modeling of the ground water seepage and stability of the initial slope

Seepage modeling

In order to evaluate the pore water pressures present before the landslide, a steady-state seepage model of groundwater conditions was performed using Seep/W (Krahn 2004a). A simplified geometry of the slope before the landslide was estimated according to cross-section B-B’ shown in Figure 8. The stratigraphy of the slope was estimated according to the data obtained from CPTU at location 32060 and from boreholes and CPTUs performed around the landslide (Figures 3 and 10). Hydraulic conductivity values used for each soil unit are presented in Table 1. They are based on values measured in the laboratory and also on vertical hydraulic gradient, observed in situ at some distance from the crest of the slope at location 32146 (Figure 13), larger in units C and D than in unit B. Modeling was performed using triangular elements having an average width of 1 m. The right, left, and bottom boundaries were considered impervious and the slope itself was considered to be a potential seepage face. The water elevation in the river was fixed at an elevation of 7 m (1 m above the bottom of the river bed). An infiltration rate of 4×10^{-10} m/s (1% of the normal annual precipitation observed in the area) was imposed on the top flat part of the slope. This infiltration rate was chosen so the modeled pore pressures would be similar to the measured piezometer pore pressures at locations 32100, 32145, and 32146.

The seepage model shows that the hydraulic head in the till under the clay deposit reaches an elevation of about 18.5 m at the level of the river, similar to the one observed in unit E at location 32145 (see Figure 13). This represents water column of about 12.5 m above the bottom of the river. Considering a water level in the river at an elevation of 7 m, this represents an upward average gradient of around 0.7 over the clay deposit between the till unit and the river bed. This results in very low effective stresses and shear strength values near the foot of the slope. The long-term stability of the initial slope was analysed using these modeled pore water pressures and SLOPE/W.

Stability analysis

Stability analyses were performed with SLOPE/W (Krahn 2004b) coupled with SEEP/W in drained conditions in order to evaluate the long-term stability of the slope and in undrained conditions as well to evaluate the safety factor for the observed failure surface.

The shear strength parameters used in the drained stability analysis are based on preconsolidation pressure, as suggested by Lefebvre (1981). Cohesion and friction angle values used for each unit are presented on Table 1. The grid and radius method was used in SLOPE/W to determine the critical failure surface in drained conditions that gives an indication of the long term stability of the slope. The critical failure surface and its corresponding safety factor are presented on Figure 15. It can be seen that the critical failure surface involved the bottom half of the slope (up to elevation 17.5 m), almost reaching the top of unit C, and has a safety factor of 0.99 with Bishop method (1.03 with Morgenstern-Price method). It also goes below the river bed. This analysis shows the precarious stability of the slope before the event of 2010.

It is believed that the spread itself occurred in a matter of a few minutes (Locat et al. 2016). It can therefore be assumed that the observed failure occurred in undrained conditions. An undrained analysis was therefore performed to evaluate the safety factor for the entire failure surface observed on site. The strength profile obtained from the field vane shear tests at location 32100 (see Figure 10) was used for this undrained analysis in SLOPE/W and the fully specified SLOPE/W option used to define the failure surface observed on site. The resulting safety factor obtained from this analysis is 2.16, with the Bishop method (2.26 with Morgenstern-Price method). Therefore, this analysis cannot explain the entire event that occurred in 2010 at Saint-Jude. It shows the limits of the usual limit equilibrium method and indicates that another calculation method is needed to explain the observed landslide and its failure mechanism.

Landslide detailed description

Morphology of the landslide

Analysis of the aerial photographs presented on Figure 3 enabled to determine the size of the landslide. Using definitions from Cruden and Varnes (1996), the width of the displaced mass is about 275 m, the length of the zone of depletion is about 150 m and the total length of the landslide is about 210 m (Figure 3). The surface of the scar itself is about 42 000 m^2

and the total area affected by the landslide (delimited by the full black line) is about 53 500 m^2. The maximum retrogression of the landslide, taken from the crest of the initial slope to its backscarp, is approximately 80 m. The position of the failure surface, as described above, made it possible to calculate a total volume of displaced material of about 520 000 m^3. The debris blocked the Salvail River and moved onto the opposite bank over a distance of about 60 m. There was no significant movement of the debris up-stream or down-stream of the Salvail River.

Traces of the initial river bed, including fresh water mussels' shells and recent river deposit, were found 50 m from their original position near the toe of the landslide (at its north-west boundary). In addition, CPTUs performed along cross-section B-B' (Figure 8) near the initial Salvail River location show that the failure surface passed below the Salvail River. These observations indicate that the failure surface came up at the ground surface on the west side of the Salvail River. Soil located near the north-west limit of the landslide therefore corresponds to soil from the initial river bed that was pushed and uplifted from elevation 6 m to elevation 15 m onto the opposite side of the Salvail River during the landslide.

The debris of the landslide can be divided into four different zones based on the observed morphology. Delimitation of these zones is shown on Figures 3, 8 and 9 by dashed lines. Zone 1 is a highly fissured area in which parts of the initial river bed were observed, mainly at its north-west border. Zone 1 is approximately 22% of the total landslide area. As explained above, soil in this zone corresponds to the initial Salvail River bed and banks that were pushed above the opposite side of Salvail River.

Zone 2 is an area with a few fissures and vegetation that was generally intact. The ground surface is roughly horizontal and trees were still standing, slightly inclined toward the backs carp of the landslide. As shown on to Figures 3, 8 and 9, zone 2 is about 20% of the total landslide area and lies on top of the Salvail River initial location and bottom of the initial slope. Observations of displacement vectors of some debris located on aerial photographs before and after the landslide indicates that the soil in this zone was initially from the upper two thirds of the initial slope that was pushed above the Salvail River's initial location in a continuous movement that kept the soil relatively intact.

Zone 3 is a highly fissured area where the ground dislocated in several blocks. A part of this zone can be observed on the upper left of Figure 4. Some of the blocks in this zone have flat tops covered with intact vegetation and other blocks are prisms with tips pointing upward. As explained above, these blocks are respectively called grabens and horsts. Figure 6 presents a photograph of a horst and a graben at the boundary between zones 3 and 4, near the house. As can be observed on Figures 8 and 9, spacing and inclination of fissured as well as the presence of vegetation on top of some horsts in zone 3 make it difficult to distinguish horsts from grabens in this zone. Stratigraphy in these blocks is generally close to the horizontal, indicating that they did not rotate during the landslide. These blocks moved over a distance of 20 to 40 m towards the Salvail River and subsided by about 8 m. This zone forms approximately 24% of the landslide area. From displacement vectors, it can be assumed that soil in zone 3 is was near the crest and the first 20 m of the top of the initial slope (see Figure 8b).

Zone 4 is an area formed of soil that was dislocated into horsts and grabens forming sub-parallel stripes oriented perpendicular to the direction of the landslide movement. Part of this zone located in the south part of the landslide is presented on the left of Figure 4. In this zone, grabens are well defined by their flat tops covered with vegetation or pieces of the road. Horsts form ridges of clay with sides inclined at around 60° (varying between 45 and 80°). Figure 5 shows a good example of a horst and a graben from zone 4. As can be observed on the horst on Figure 5, stratifications inside horsts were inclined between 0 and 17° with the horizontal (see also Figures 8a and 9a), indicating that these blocks did not rotate much during the movement. It was also observed that the downstream side of some horsts was covered with brown soil, thus coming from the sandy crust and contrasting with the grey clay (unit B) forming them. This last observation was also noted by Carson (1979a), on the 1978 landslide at Rigaud, and by Geertsema et al. (2006), on the Mink Creek landslide. In addition to horsts and grabens, slices of soil, originally horizontal, were found inclined after the movement at an angle of 25 to 50° with respect to the horizontal (see Figures 8a and 9a). These slices were observed directly behind some horsts. At some other places, inclined slices had slid over grabens in front of them, as seen on Figure 7. These slices were also observed at the base of grabens located near the backscarp of the landslide. Such slices have rarely been observed or at least reported for this type of landslide, except in the case of the 1978 Sainte-Madeleine-de-Rigaud spread described by Carson (1979a) and at Mink Creek in British Columbia (Geerstema 2004). Soil in zone 4 is soil that was initially between the initial location of the house and the backscarp of the landslide. Zone 4 covers about 34% of the total landslide area.

Characteristics of the debris

Four trenches were dug into horsts and inclined slices in order to observe their stratifications and understand their formation (see Figure 3 for location). Figure 16 shows a photograph of the trench at location 32152, close to cross-section C-C' (see Figures 3 and 9a for location) and inclined slices shown on Figure 7, that has been observed in details. It can be seen that the trench has exposed close 3 m of the top if these inclined slices (on the left side of Figure 16) and a horst (on the right side of Figure 16) in the direction perpendicular to the general ground movement. The two types of structure are easily differentiated by the inclination of their stratifications. The stratifications of the horst are inclined of about 10° to the horizontal whereas the stratifications of the slices are inclined close to 50° to the horizontal. The contact between the horst and the slices has an angle of about 70° to the horizontal. This angle as well as the inclination of the stratification indicates that this horst has been rotated by about 10°. The different slices have a thickness of about 60 cm each with several of them outcropping side by side immediately behind the horst. They were separated by shear zones made up of silty soil, having a thickness close to 2 mm, and following stratification.

CPTUs and boreholes at locations 32140 and 32141 (see figures 17 and 18 respectively) were performed through the inclined slices near the trench at location 32152, shown on Figure 16. Water content was also measured on soil samples at various depths from these boreholes. In addition, these samples were passed through CAT scan to obtain images of the stratifications of the intact soil. Each profile also presents the description of soil units, the water content profile, the undrained shear strength interpreted from CPTU, and the location of the failure surface. Readers should refer to Locat et al. (2011b) for further detail about these boreholes.

Results from location 32140 (Figure 17) show that the failure surface is located at a depth of 17.3 m (elevation 3.5 m). Debris at this location are represented by unit F subdivided into 5 subunits: F1, F2, F3, F4, and F5. Subunit F1 (from the ground surface down to a depth of 5.1 m) is a soft silty clay with stratifications inclined at about 45° to the horizontal. The average water content of this subunit is about 65%, typical of unit B on Figure 10, and the shear strength varies from 16 to 27 kPa with depth. This subunit corresponds to the inclined slices observed from the ground surface (see figure 13). From a depth of 5.1 m down to a depth of 8.6 m, a stiff grey-brown sandy and silty layer is observed (subunit F2). CAT scan shows that stratification in this subunit is slightly inclined. The average water content is 29% and shear strength has values between 50 to 200 kPa. These characteristics are typical of the sandy crust observed in intact soil (unit A on Figure 10). Underneath, lays a very soft grey clayey silt having inclined stratifications from depths 8.6 to 11.6 m, becoming more clayey at a depth of 11 m (subunit F3). The water content of this subunit varies from 24 to 70% and the shear strength is around 3 kPa. A soft grey silty clay with inclined and folded stratification was found from depths of 11.6 to 12.8 m (subunit F4). The average water content is 62% and shear strength varies from 24 to 30 kPa with depth. Geotechnical properties of this subunit indicate that it is soil from unit B that was sheared during the landslide. Stiff grey silty clay with horizontal stratifications (subunit F5) is found below a depth of 12.8 m down to the failure surface observed at a depth of 17.3 m. The water content in this subunit is generally constant with an average value of 65%. The shear strength varies from 45 to 65 kPa with depth. These characteristics are typical of the soil from unit B on Figure 10 that was involved in the landslide. Below the failure surface units B, C, and D, also detected in the intact deposit (Figure 10), are observed. They exhibit properties similar to those observed at locations 32092 and 32100, indicating continuity in the stratigraphy of the deposit.

Results from location 32141 (Figure 18) show that the failure surface is located at a depth of 16.9 m (elevation 3.7 m). Debris (unit F) at this location can be divided in three subunits: F1, F4 and F5 (Figure 18). A soft grey silty clay with stratification inclined at about 45° to the horizontal is observed from the ground surface down to a depth of 9.8 m. Its water content is 62% in average and the shear strength varies from 17 to 39 kPa. Around a depth of 9 m, the shear strength decreases down to about 3 kPa. This subunit presents similar properties with subunit F1 at location 32140 (Figure 17) and originates from unit B. It corresponds to inclined slices observed at the ground surface. Grey stiff soft silty clay with folded and disturbed stratifications is observed from a depth of 9.8 m to a depth of 10.6 m. A sample from this subunit shows almost vertical stratifications. The average water content is 65% and the shear strength of the soil varies from 40 to 50 kPa. The properties of this subunit correspond to soil from unit B (Figure 10) that was sheared during the landslide and are comparable with subunit F4 from location 32140 (Figure 17). From 10.6 m down to the failure surface, at a depth of 16.9 m, a stiff grey silty clay with horizontal stratifications is observed. The average water content of this subunit is 65% and its shear strength varies from 50 to 70 kPa with depth. The properties of this subunit are similar to those observed for unit B (Figure 10), involved in the landslide and are similar to those of subunit F5 (Figure 17). Below the failure surface Units B, C and D have been observed and represent the intact soil under the landslide body.

CPTU 32120 was performed through the horst exposed by trench at location 32152 and shown on Figure 16, near location 32140 (see Figure 3). Figure 19 shows the results of this in situ test. At this location, the failure surface is at a depth of 16.8 m (elevation 3.8 m) and the debris (unit F) can be divided in three subunits: F6, F2 and F3. It can be seen that for the first 3 m, the corrected tip resistance and the pore pressure are about 400 kPa and 200 kPa respectively, indicating a clayey soft layer. This indicates that this subunit F6 corresponds to the horst observed at the ground surface (Figure 16). From a depth of 3 m to a depth of 8 m, the corrected tip resistance varies from 550 kPa to more than 3000 kPa and the pore pressure is closed to 0 kPa. This indicates a stiff coarse layer very similar to the sandy crust observed at location 32140 (subunit F3 on Figure 17). From a depth of 8 m down to a depth of 16.8 m (depth of the failure surface), the soil is a grey silty clay and the corrected tip resistance varies between 300 to 600 kPa. Under the failure surface the intact soil, observed at location 32100 (Figure 10) is also detected and corresponds to units B, C and D as observed at location 32100.

Figure 20 shows location of profiles 32120, 32140 and 32141 (Figures 17 to 19) on part of cross-section C-C' (see Figure 9), and examples of CPTU and CAT scan images obtained at location 32140. A schematic cross-section of the trench and location of these soundings is also shown in figure 20. Extrapolating the subunits observed at locations 32120, 32140 and 32141 it is possible to get an approximate interpretation of the stratigraphy near these three soundings. The top soft silty clay layer (subunit F1 on Figures 17 and 18) represents inclined slices observed at trench 32152, on Figure 16 and is originating from unit B (Figure 7). Unfortunately, this latter unit is so homogeneous in terms of water content that it is not possible to specify the original elevation of that subunit. The stiff sandy layer (subunit F2 on Figures 17 and 19) seen on profiles 32140 and 32120 represents the sandy crust of a graben (graben on the right on figure 20a). Subunit F3, observed at locations 32140 and 32120 (Figures 17 and 19), would correspond to soil below this sandy crust forming the bottom of this graben. Units F5 (Figures 17 and 18) show horizontal stratification above the failure surface that seems to correspond to the lower base of the horst. Subunit F4 (Figures 17 and 18) would correspond to a shear zone forming between the base of the inclined slices and the horst sides during the movement. The tip of that horst (observed on Figure 16 and corresponding to subunit F6 on Figure 19) could have been swept away on top of the graben by the inclined slices, creating the observed morphology.

Another CPTU, performed at location 32118 in the debris (see figure 3 for location) shown on Figure 21, presents a sandy crust (unit A as presented on figure 7) located a depth of 10 m in the debris and covered by what can be identified as a silty clay layer. This indicates that, at this location, the sandy crust, originally located at the ground surface, subsided from an elevation of 28 m down to an elevation of 10 m and was covered by other debris. This is considered to be the lowest elevation where the sandy crust is found in the debris. This detailed study shows the complexity of soil movements that occurred during the 2010 Saint-Jude spread.

Discussion on the landslide failure mechanism

Based on the 2010 Saint-Jude landslide investigation presented above, and as shown in Figure 15, the bottom half of the slope was marginally stable, which is in accordance with the observed ground movements on aerial photograph of the site taken in august 2009 (see section The landslide and its regional context). Debris of these movements were probably eroded during the 2010 spring, unloading the toe of the slope and further decreasing the overburden pressure under the river. It has to be noted that there was no witness, nor any indication that an initial slide large enough to be noted by the residents of the house could have occurred just before the main landslide. The family living on the site did not mention anything about such an event to a visitor who talked to them half an hour before the main event. It is therefore difficult to know the exact trigger of the 2010 landslide, but it can be taught that an initial instability could have developed, with time, near the toe of the slope and, given the high artesian pore pressures, reduced the vertical and horizontal stresses under the river, and initiated the main failure surface 2.5 m below the river bed elevation. From that point, the failure progressed horizontally for about 125 m in the intact deposit, as seen on Figures 8 and 9. The presence of high artesian pressure could have influenced the location of the failure surface, located 2.5 m below the river bed. However, the exact influence of such hydraulic conditions on the failure mechanism is still not clear and should be studied further in relation to spreads. These observations indicate that, most probably, the 2010 landslide seems to be of natural origin and triggered by erosion near the toe of the slope with high artesian pressures under the river, and deepening of the river with time with a process similar to that described by Lefebvre (1986).

As explained by Bjerrum (1967), Quinn et al. (2011), Locat et al. (2011a, 2013 and 2015) and Leroueil et al. (2012), progressive failure can explain how a failure surface can progress horizontally into an intact soil mass creating a spread. Locat et al. (2011a, 2013 and 2015) associated the development of spreads in sensitive clays with progressive failure by two distinct processes: (i) propagation of the failure surface horizontally into an intact soil mass and (ii) dislocation of the soil mass above the failure surface into horsts and grabens. As explained by Leroueil (2012), development of progressive failure requires: (i) a geomaterial with strain softening behaviour; (ii) non-uniformity of stresses; (iii) boundary conditions enabling the slope to deform; and (iv) stresses exceeding the peak shear strength of the soil. The present study demonstrates that the Saint-Jude landslide corresponds to all of these criteria: (i) the clay involved in the landslides presents a strain-softening behaviour during shear (see Figures 11 and 12); (ii) shear stresses were present in the slope, giving the initial slope inclination; (iii) the soil mass involved in the landslide was free to move towards the opposite river bank; and (iv) the initial slope was unstable, as demonstrated by the stability analysis taking into account the high hydraulic gradient under the river. It is also probable that the shear stresses were larger than or closer to the peak shear strength of the soil near the toe of the slope (Figure 15). Conditions for progressive failure seem therefore to have been present and progressive failure could have taken an important role in the initiation and propagation of the main failure surface. In addition, Locat et al. (2011a, 2013 and 2015) explained and demonstrated that when progressive failure is taken into account to understand spreads in sensitive clays, only a small unloading near the toe of the slope can initiate a failure surface resulting in a spread. As mentioned above, it is not clear what was the importance of the trigger necessary to initiate the 2010 Saint-Jude landslide. It can be said that, as the safety factor of the initial slope was low, the magnitude of the trigger did not need to be large in order to initiate the main failure surface under the river bed.

Giving the detailed study of the morphology of this landslide, it was possible to reconstruct the initial and final conditions of the debris and understand better the dislocation mechanism that occurred during this spreads. Figure 22 presents cross sections A-A’, B-

B' and C-C' before and after the landslide, showing the probable initial and final position of the debris. The final positions of horsts presented in Figures 22b, d and f were determined from field observations and correspond to horsts presented on Figures 8 and 9. Locations of sandy crust and parts of horsts B-2 and C-3 that are below the ground surface after the landslide were determined by careful study of soundings performed inside the landslide as described in section Characteristics of the debris. The initial probable positions of horsts presented in Figures 22a, c and e were estimated with the help of the displacements vectors of targets shown in Figures 8 and 9 (further details on displacement vectors are given in Locat et al. 2011b) and by assuming that (i) horsts had tip angle of 60° (see Locat et al. 2011a) and (ii) that they only translated during the movement with no subsidence, keeping their initial shape.

From Figure 22, it can be interpreted, that once the main failure has been formed inside the intact deposit, the entire soil above moved horizontally towards the river and the bottom of the river was pushed over the opposite bank. This created morphological zones 1 and 2 (Figures 3, 8 and 9). As the failure surface continued its progression, the above soil mass dislocated in horsts (A-1, A-2, B-1, B-2, C-1, C-2 and C-3 on Figure 22) and grabens observed in zone 3 (Figures 3, 8 and 9). This first phase of the movement seems to have stopped behind the house, as seen on Figures 8 and 22, were the failure surface gets at a higher elevation of 14 m. Stratifications in horsts are inclined between 0 and 15° with the horizontal, which corresponds to stratifications in intact soil. This indicates that horsts moved mainly horizontally with only minor rotation during the landslide. The presence of these horsts enables to classify this landslide as a spread. In addition, inclinations of horsts' sides are inclined at about 60° to the horizontal. This inclination corresponds to the results of an active failure, as seen in undrained triaxial tests on clay. Horsts seem therefore to be formed by active failure occurring during the landslide as explained by Locat et al. (2011a, 2013 and 2015).

Looking at Figure 22, it can be seen that horsts A-1, A-2, B-1, C-1 and C-2 have moved toward the initial position of the river and were compressed against the debris from zone 1 and 2 stopped on the opposite bank. It can also be seen that for each cross-section, sandy crust on top of grabens behind horsts A-2, B-1 and C-2 were found deep in the debris at level of soundings 32118 (Figure 21), 32119, 32120 (Figure 19) and 32140 (Figure 17) and covered with debris from horsts A-3, B-2 and C-3 located behind them. This indicates that grabens behind these horsts subsided, probably allowing overtopping when horsts B-2 and C-3 moved toward the river and were stopped by the lower downstream debris. It seems that the movement was fast enough for the tips of horsts B-2 and C-3 to be disconnected from their base and move over the lower graben as presented in Figures 16, 20, 22d and f and explained in section Characteristics of the debris, creating zone 3.

An unstable scarp, creating the appropriate conditions for the upper failure surface to form 10 m higher than the first one (see Figures 8, 9, 21, and 22), seems to have formed after the first phase of the movement creating zones 1 to 3. It is not clear how this upper failure surface was formed, but progressive failure was probably also involved in this failure. As this upper failure propagated, horsts A-3, A-4, A-5, B-3 and C-4 (Figure 22) and grabens were formed. This part of the debris was delimited as zone 4 in Figures 3, 8 and 9. From Figure 22, it can be observed that inclined slices found in this zone were formed as a result of overlapping movement of graben tops when this soil mass slid on top of downstream debris. It is not exactly clear how the upper failure surface and inclined slices have formed, but reconstitution of the movement in Figure 22 explains observations near trench 32152 showing how inclined slices and horst tips moved on top of grabens and, in doing so, crushed the house basement and indicating that the kinetic energy of the landslide was very high.

Conclusion

The 2010 landslide at Saint-Jude has been very well documented. The stratigraphy and the geotechnical properties were found to be uniform around the landslide. The soil involved in the landslide mainly consists of sensitive grey clay typical of Champlain Sea Clay, with liquidity index varying from top to bottom between 2 to 1, intact shear strength increasing linearly with depth from 25 to 65 kPa and an OCR decreasing over the same depths from 1.9 to 1.2. The important points resulting from the investigation of the landslide are:

- River erosion and high artesian pore pressures under the river seem to have been aggravating factors decreasing the stability of the initial slope.
- It is believed that the Saint-Jude landslide could have been triggered by natural causes. The magnitude of the triggering event that initiated this landslide is however not known, but could have been small given the low stability of the initial slope.
- The failure surface was identified with CTPUs tests. It started 2.5 m under the river elevation and propagated almost horizontally over 100 m in the intact deposit.
- The initial slope moved over the opposite side of the river with only a little disturbance in the debris. Behind it, the soil mass dislocated in several blocks, having horst and graben shapes.

- An upper failure surface, about 10 m higher than the main one was also located with CPTUs. This seems to indicate that the movement has occurred in two successive phases, along two failure surfaces at different elevations. This is one of the first time that two failure surfaces are clearly observed in a spread.
- Stratifications in horsts indicate that the main movement of the debris was mostly translational along the failure surface, with little or no rotation. This indicates that the landslide did not occur as the result of a succession of rotational slides, which would have induced more rotation of the debris and might not have led to the formation of a continuous failure surface.
- Another rare particularity of this landslide is the presence of inclined slices observed in the upper part of the debris. These inclined slices could result from the rotation of the bottom part of some grabens sliding along the upper failure surface onto the debris from the lower failure surface.
- Reconstitution of the initial position of the debris allowed the understanding of the dislocation of the debris and showed the complexity of the 2010 Saint-Jude spread.

The investigation of the Saint-Jude landslide gives valuable information on the mechanisms and kinematics of spreads occurring in sensitive clays, which are very different from other types of retrogressive landslides such as flowslides. It also emphasizes the need of detailed investigations in order to understand the conditions of initiation and development of spreads.

Acknowledgments

The authors would like to acknowledge the precious collaboration of Saint-Jude municipal authorities, particularly Mayor Yves de Bellefeuille and General Director Sylvie Beauregard. Sincere thanks to the family of the people that lost their life in this tragic event and also to the Saint-Jude citizens for their essential collaboration during this investigation. Without their assistance, this work would not have been possible.

Many people at the MTMDET need to be acknowledged for their contribution to this work, in particular: Martin D’Anjou, Thomas Fournier, Gilbert Grondin, Denis Hudon, Daniel Ouellet and Mélissa Raymond. Finally, the authors would also like to recognize François Noël for realizing, as an MTMDET intern, detailed cross-sections of the landslide presented in this paper and Sandra Veillette, a master student, for the help with some figures used in this paper. Dr. Pete Quinn and another anonymous reviewer are acknowledged for their constructive comments.

References

Bjerrum, L. 1967. Progressive failure in slopes in overconolidated plastic clay and clay shales. Terzaghi Lecture. Journal of the Soil Mechanics and Foundations Division, ASCE, **93**(5): 3-49.

Carson, M. A. 1979a. *Le glissement de Rigaud (Québec) du 3 Mai 1978: Une interprétation du mode de rupture d’après la morphologie de la cicatrice*. Géographie physique et Quaternaire, **33**(1): 63-92.

Carson, M. A. 1979b. *On the retrogression of landslides in sensitive muddy sediments: Reply*. Canadian Geotechnical Journal, **16**(2): 431-444.

Cruden, D. M., and Varnes D. J. 1996. *Landslides types and processes*. In Landslides investigation and mitigation, Special Report 247, Transportation, Research Board, National Research Council, Edited by A. K. Turner, and R. L. Schuster, National Academy press, Washington, D.C. pp. 37-75.

Demers, D., Robitaille, D., and Perret, D. 2000. *The St. Boniface Landslide of April 1996 : a Large Retrogressive Landslide in Sensitive Clay with Little Flow component*. In Proceedings of the 8th International Symposium on Landslides, Cardiff, 26-30 June 2000. Thomas Telford Publishing, London, Vol. 1, pp. 447-452.

Geertsema, M., Cruden, D. M., and Schwab, J. W. 2006. *A large landslide in sensitive glaciomarine sediments at Mink Creek, northwestern British Columbia, Canada*. Engineering Geology, **83**(1-3): 36-63.

Geertsema, M. 2004. *A composite earthflow-spread in sensitive glaciomarine sediments near Terrace, British Columbia*. M.Sc. thesis, University of Alberta, 147 pp.

Grondin, G. and Demers, D. 1996. *The Saint-Liguori flakeslide: Characterisation and remedial works*. *In* Proceedings of the 7th International Symposium on Landslides, Trondheim, Norway, 17-21 June 1996. *Edited by* K. Senneset. Balkema, Rotterdam, the Netherlands. Volume 2, pp. 743-748.

Hungr, O., Leroueil, S., and Picarelli L. 2014. *The Varnes Classification of landslide types, an update*. Landslides, **11**(2): 167-194.

Krahn, J. 2004a. Seepage modeling with SEEP/W, an engineering methodology. GEO-SLOPE International, Ltd., Calgary, Alta.

Krahn, J. 2004b. Stability modeling with SLOPE/W, an engineering methodology. GEO-SLOPE/W International, Ltd., Calgary, Alta

Lefebvre, G. 1986. *Slope instability and valley formation in Canadian soft clay deposits*. Canadian Geotechnical Journal, **23**(3): 261-270.

Lefebvre, G. 1981. *Fourth Canadian Geotechnical Colloquium: strength and slope stability in Canadian soft clay deposits*. Canadian Geotechnical Journal, **18**(3): 420-442.

Leroueil, S., Locat, A., Eberhardt, E., and Kovacevic, N. 2012. Keynote Lecture: *Progressive failure in natural and engineering slopes*. *In:* EBERHARDT E. et al. (eds) Landslides and Engineered Slopes: Protecting Society through Improved and Understanding. Proceedings of the 11th International and 2nd North American Symposium on Landslides, 3-8 June 2012, Banff, Alberta. Taylor & Francis Group. pp. 31-46.

Leroueil, S., Tavenas, F., and Le Bihan, J.-P. 1983. *Propriétés caractéristiques des argiles de l'est du Canada*. Canadian Geotechnical Journal, 20(4): 681–705.

Locat, A., Demers, D., and Leroueil, S. 2016. *Spreads in Canadian sensitive clays. In:* AVERSA, S. et al. (eds.) Landslides and Engineered Slopes – Experience, Theory and Practice. Proceedings of the 12th International Symposium On Landslides. 12-19 June 2016, Napoli, Italy. Taylor & Francis Group. pp. 1295-1304.

Locat, A., Leroueil, S., Bernander, S., Demers, D., Jostad, H. P., and Ouehb, L. 2011a. *Progressive failures in Eastern Canadian and Scandinavian sensitive clays*. Canadian Geotechnical Journal, **48**(11): 1696-1712.

Locat, A., Leroueil, S., Bernander, S., Demers, D., Locat, J., and Ouehb, L. 2008. *Study of a lateral spread failure in an eastern Canada clay deposit in relation with progressive failure: The Saint-Barnabé-Nord Slide*. In Proceedings of the 4th

Canadian Conference on Geohazards: From Causes to Management. Québec, Que., 20-24 May 2008. Edited by J. Locat, D. Perret, D. Turmel, D. Demers et S. Leroueil, Presses de l'Université Laval, Québec, Que. pp. 89-96.

Locat, A., Leroueil S., Locat P., Demers D., Robitaille, D., et Lefebvre, G. 2012a. *In Situ Characterisation of the Saint-Jude landslide, Québec, Canada*. In the Proceedings of the 4th International Conference on Geotechnical and Geophysical Site Characterisation, ISC'4, 18-21 September, 2012, Porto de Galinhas, Brazil. Vol. 1, pp. 507-514.

Locat P., Demers D., Robitaille D., Fournier T., Noël F., Leroueil S., Locat A., et Lefebvre G. 2012b. *The Saint-Jude landslide of May 10, 2012, Québec, Canada*. *Dans* Eberhardt, E. et al. (eds) Landslides and Engineered Slopes: Protecting Society through Improved and Understanding. Proceedings of the 11th International and 2nd North American Symposium on Landslides, 3-8 June 2012, Banff, Alberta. Taylor & Francis Group. pp. 635-640.

Locat, P., Fournier, T., Robitaille, D., and Locat, A. 2011b. *Glissement de terrain du 10 mai 2010, Saint-Jude, Montérégie, Rapport sur les caractéristiques et les causes*. Rapport MT11-01. Section des mouvements de terrain, Services de la géotechnique et de la géologie, Ministère des transports du Québec. Bibliothèque et Archives nationales du Québec, Gouvernement du Québec. 101 p.

Ochietti, S. 1989. *Quaternary geology of St. Lawrence Valley and adjacent Appalachian subregion*. In: Fulton, R.T. (ed.), Quaternary Geology of Canada and Green-land, Geological Survey of Canada, Geology of Canada, 1 (also: Geological Society of America, The Geology of North America, K-1), 350-379.

Odenstad, S. 1951. *The landslide at Sköttorp on the Lidan River, Frebruary 2, 1946*. Royal Swedish Institute Proceedings, **4** :1-40.

Quinn, P.E., Diederichs, M.S., Rowe, R.K. and Hutchinson, D.J. 2011. A new model for large landslides in sensitive clay using a fracture mechanism approach. Canadien Geotechnical Journal, **48**(8)L 1151-1162.

Rissmann, P., Allard, J.-D., and Lebuis, J. 1985. *Zones exposées aux mouvements de terrain le long de la rivière Yamaska, entre Yamaska et Saint-Hyacinthe*. Ministère de l'Énergie et des Ressources, Rapport DV 83-04.

Tavenas, F. 1984. *Landslides in Canadian sensitive clays - a state-of-the-art*. *In* Proceedings of the 4th International Symposium on Landslides, Toronto, Ont., 16-21 September 1984. University of Toronto Press, Toronto, Ont. Volume 1, pp. 141-153.

TABLE AND FIGURE CAPTIONS

Table 1: Input parameters for seepage modeling and stability analysis.

Figure 1 : Location of the 2010 landslide at Saint-Jude. Dark grey area shows the extent of the Champlain Sea deposit in Quebec.

Figure 2 : Digital elevation model of the region obtained from LIDAR surveys, showing the numerous scars of interpreted previous landslides (dashed line) and the 2010 event. Water flow in the Salvail River is from south to north.

Figure 3 : Aerial view of the landslide at Saint-Jude taken on May 11th 2010, the day after the landslide while excavation work were going on near the house (Courtesy of MTMDET). Location of the soundings, delimitations of the landslide and its morphological zones as well as the crest of the slope are shown. Note that the crest of the slope inside the landslide footprint is the estimated crest of the slope location before the landslide. Movement direction of the debris is toward the Salvail River, at the top of the photograph.

Figure 4: General photograph of the south part of the landslide taken on May 11th 2010, the morning after the landslide. Movement direction is toward the top left of the photograph (Courtesy of MTMDET).

Figure 5 : Photograph of a horst and a graben close to section B-B’ (see Figure 3), taken on May 18th 2010, eight days after the landslide (modified from Locat et al. 2012a).

Figure 6: View of a graben and a horst behind the house, close to section B-B' (see Figure 3) taken on May 11th 2010, the morning after the landslide (Courtesy of MTMDET). Movement direction is toward the left of the photograph.

Figure 7: Closer view of the south part of the landslide, close to section C-C' (see Figure 3), showing inclined slices (Courtesy of MTMDET). Movement direction is toward the right of the figure. Photograph taken on May 11th 2010, the morning after the landslide.

Figure 8 : Cross-section B-B'. (a) 3 times vertical exaggeration and (b) to scale (see Figure 3 for location of cross-section, modified from Locat et al. 2012b).

Figure 9 : Cross-section C-C'. (a) 3 times vertical exaggeration and (b) to scale (see Figure 3 for location of cross-section, modified from Locat et al. 2012a).

Figure 10 : Geotechnical profile at location 32100 outside the footprint of the 2010 landslide (see Figure 3 for location). Where w_{cone} is fall cone test water content used to calculate I_L, $w_{natural}$ is the natural water content, I_P the plasticity index, σ'_{pCPTU} the σ'_p estimated with CPTU, $N_{\sigma t}$ a dimensionless parameter for σ'_{pCPTU}, and σ'_v the vertical effective stress calculated with pore water pressure from piezocone at location 32100 (u_{Z32100}).

Figure 11 : Results of a triaxial undrained compression tests consolidated under an effective stress (σ'_c) of 87 kPa on a sample taken at a depth of 22.2 m from the borehole at location 32092.

Figure 12 : Results of constant volume DSS tests (a) consolidated under an effective stress of 90 kPa on a sample taken at a depth of 22.1 m and (b) consolidated under an effective stress of 170 kPa on a sample taken at a depth of 22.7 m, both at location 32092.

Figure 13 : Cross-section D-D’, view toward the north, piezometers at location 32145, 32100 and 32146 (see Figure 3 for locations, modified from Locat et al. 2012a).

Figure 14 : Failure surface identified by CPTU (see Figure 3 for location of CPTUs.

Figure 15 : Result of the drained stability analysis showing the critical failure surface (dashed line) and grey zone locating failure surfaces giving a safety factor lower than 1.05.

Figure 16 : View toward the south-west of the trench 32152 and approximate location of sites 32120, 32140 and 32141 (see Figures 3 and 9 for location). The picture was taken on June 16th 2010, about a month after the landslide (modified from Locat et al. 2012a).

Figure 17 : Geotechnical profile at location 32140 in the debris (see Figure 3 for location).

Figure 18 : Geotechnical profile at location 32141 in the debris (see Figure 3 for location).

Figure 19 : CPTU profile at location 32120 in the debris and corresponding units as described on Figures 17 and 18 (see Figure 3 for location).

Figure 20 : a) Approximate interpretation of the stratigraphy near trench 32152 (Figures 9 and 16), view toward the south-west, including location of soundings and b) example of CPTU and CAT scan results at location 32140 (see Figures 3 and 9 for location, modified from Locat et al. 2012a).

Figure 21: CPTU profile at location 32118 in the debris showing the sandy crust, introduced on figure 10, buried at a depth 10 m under a layer of silty clay (see Figure 3 for location).

Figure 22: Drawing showing suggested position of each horst and graben before (a, c and e) and after (b, d and f) the landslides for cross-sections A-A’, B-B’ and C-C’.

Table 1: Input parameters for seepage modeling and stability analysis.

Soil unit	k (m/s)	c' (kPa)	ϕ' (°)
A	2×10^{-7}	0	35
B	9×10^{-10}	7.7	35
C	5×10^{-10}	7.7	40
D	5×10^{-10}		
E	1.5×10^{-7}		

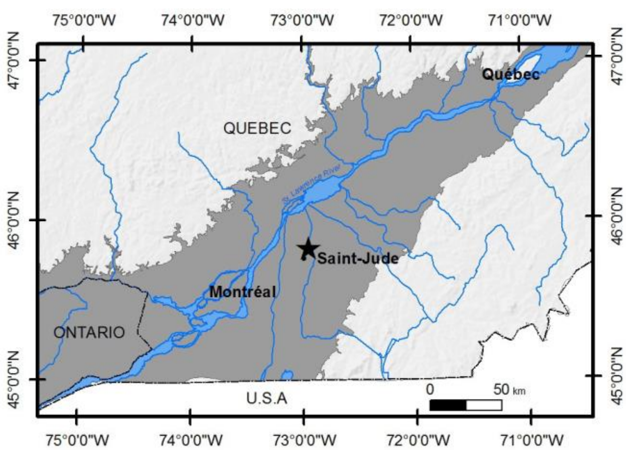

Figure 1 : Location of the 2010 landslide at Saint-Jude. Dark grey area shows the extent of the Champlain Sea deposit in Quebec.

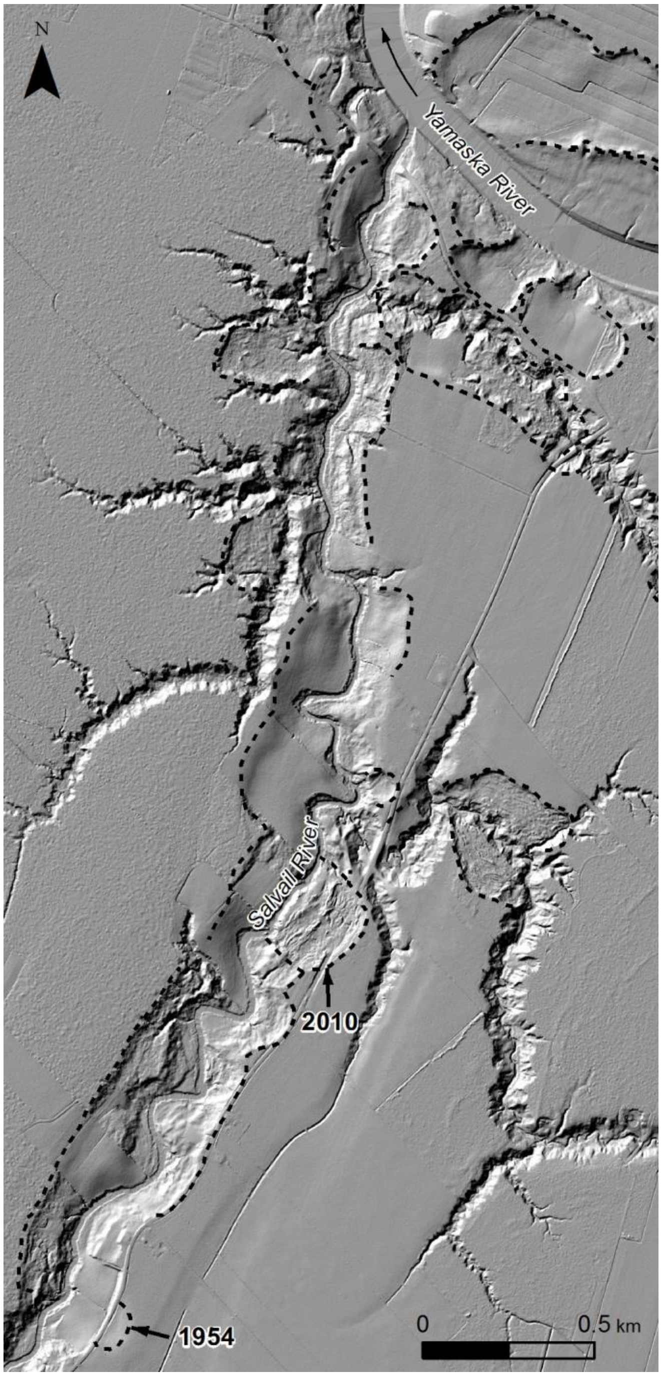

Figure 2 : Digital elevation model of the region obtained from LIDAR surveys, showing the numerous scars of interpreted previous landslides (dashed line) and the 2010 event. Water flow in the Salvail River is from south to north.

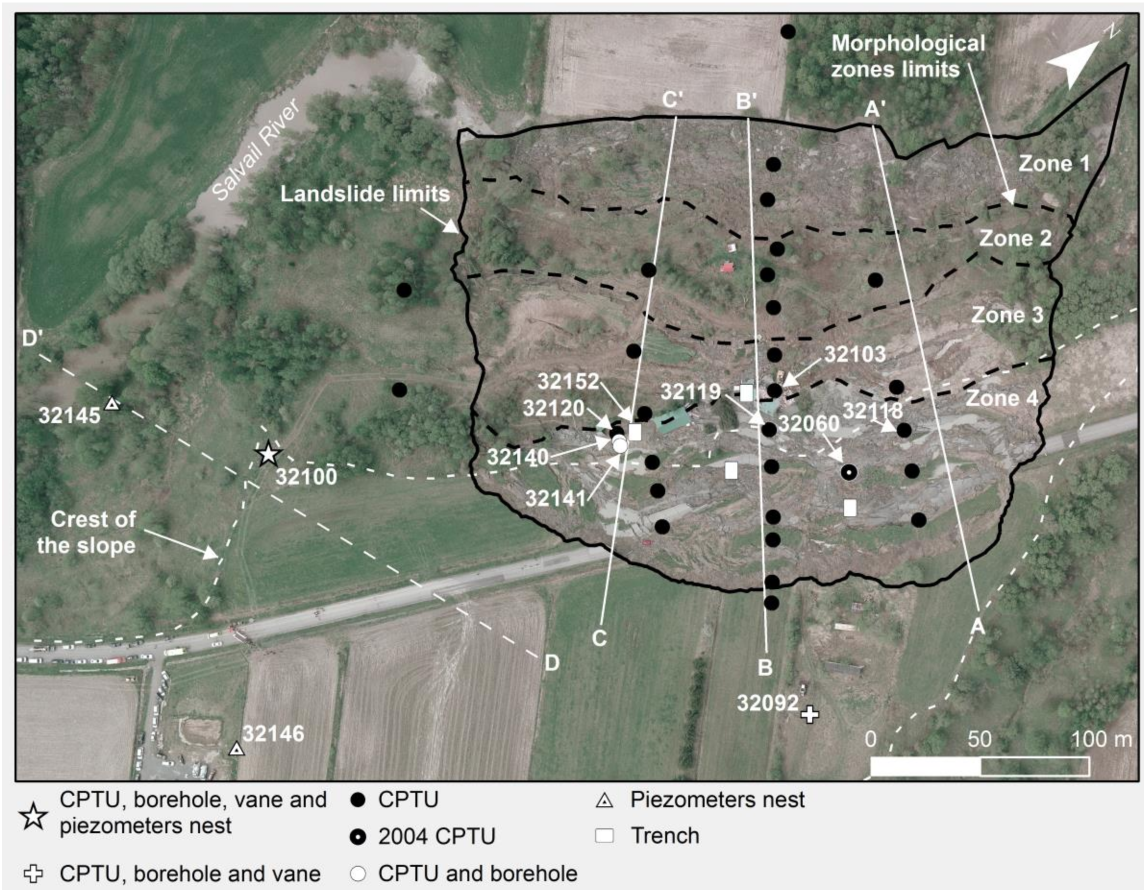

Figure 3 : Aerial view of the landslide at Saint-Jude taken on May 11th 2010, the day after the landslide while excavation work were going on near the house (Courtesy of MTMDET). Location of the soundings, delimitations of the landslide and its morphological zones as well as the crest of the slope are shown. Note that the crest of the slope inside the landslide footprint is the estimated crest of the slope location before the landslide. Movement direction of the debris is toward the Salvail River, at the top of the photograph.

Figure 4: General photograph of the south part of the landslide taken on May 11th 2010, the morning after the landslide. Movement direction is toward the top left of the photograph (Courtesy of MTMDET).

Figure 5 : Photograph of a horst and a graben close to section B-B' (see Figure 3), taken on May 18th 2010, eight days after the landslide (modified from Locat et al. 2012a).

Figure 6: View of a graben and a horst behind the house, close to section B-B' (see Figure 3) taken on May 11th 2010, the morning after the landslide (Courtesy of MTMDET). Movement direction is toward the left of the photograph.

Figure 7: Closer view of the south part of the landslide, close to section C-C’ (see Figure 3), showing inclined slices (Courtesy of MTMDET). Movement direction is toward the right of the figure. Photograph taken on May 11th 2010, the morning after the landslide.

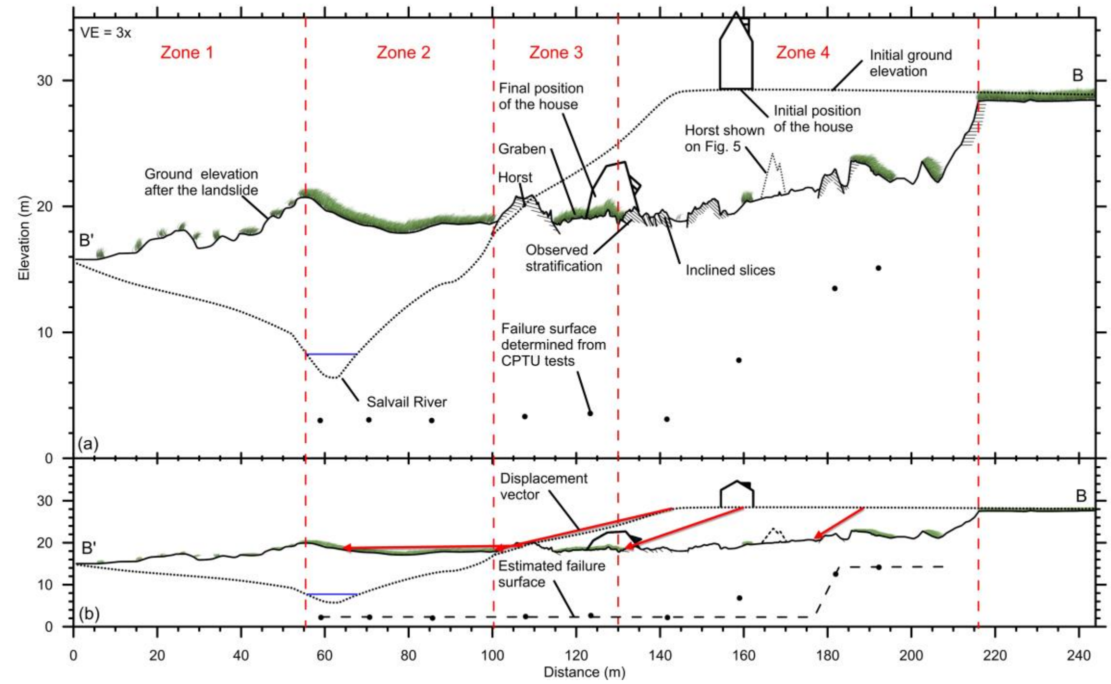

Figure 8 : Cross-section B-B’. (a) 3 times vertical exaggeration and (b) to scale (see Figure 3 for location of cross-section, modified from Locat et al. 2012b).

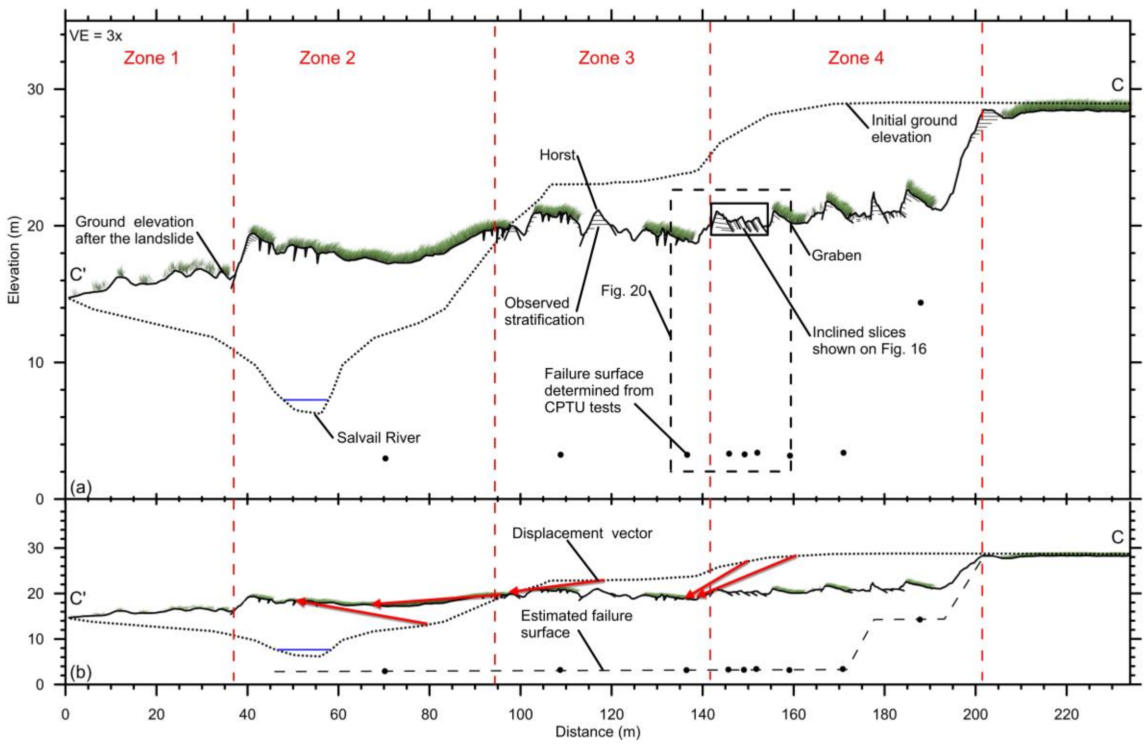

Figure 9 : Cross-section C-C'. (a) 3 times vertical exaggeration and (b) to scale (see Figure 3 for location of cross-section, modified from Locat et al. 2012a).

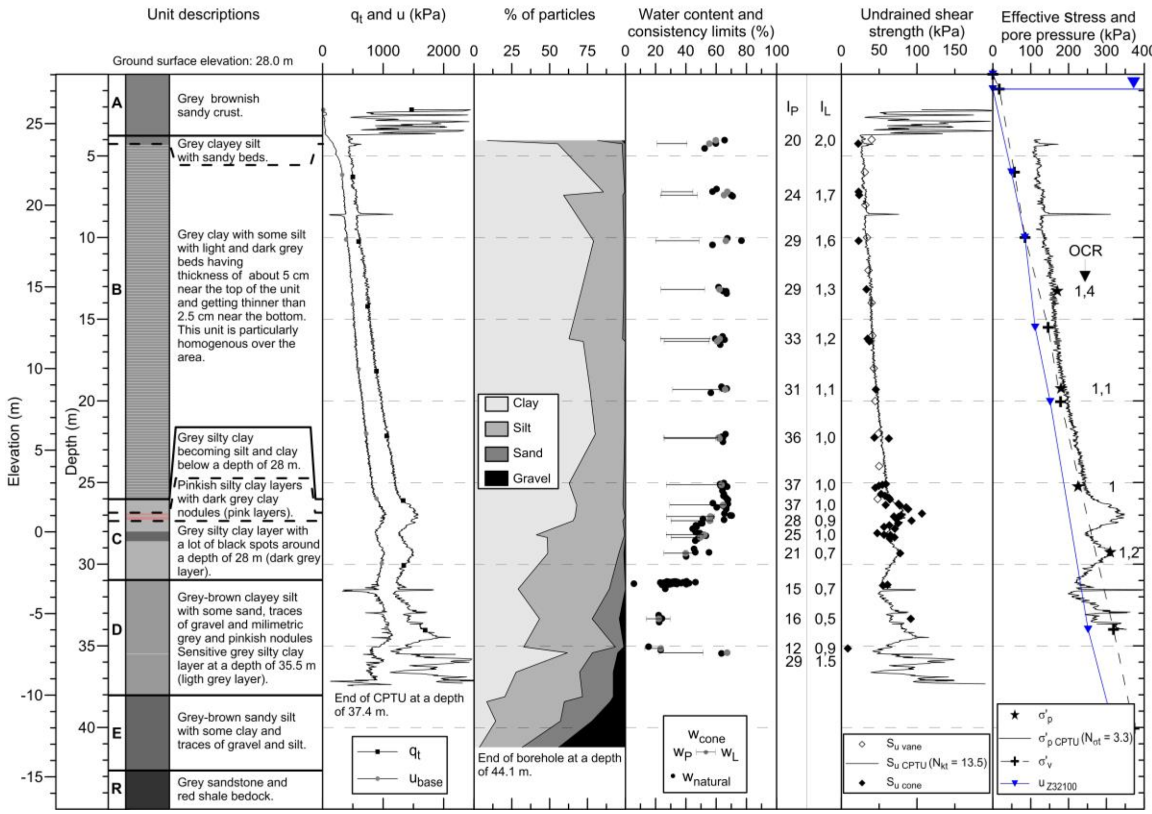

Figure 10 : Geotechnical profile at location 32100 outside the footprint of the 2010 landslide (see Figure 3 for location). Where w_{cone} is fall cone test water content used to calculate I_L, $w_{natural}$ is the natural water content, I_P the plasticity index, σ'_{pCPTU} the σ'_p estimated with CPTU, $N_{\sigma t}$ a dimensionless parameter for σ'_{pCPTU}, and σ'_v the vertical effective stress calculated with pore water pressure from piezocone at location 32100 (u_{Z32100}).

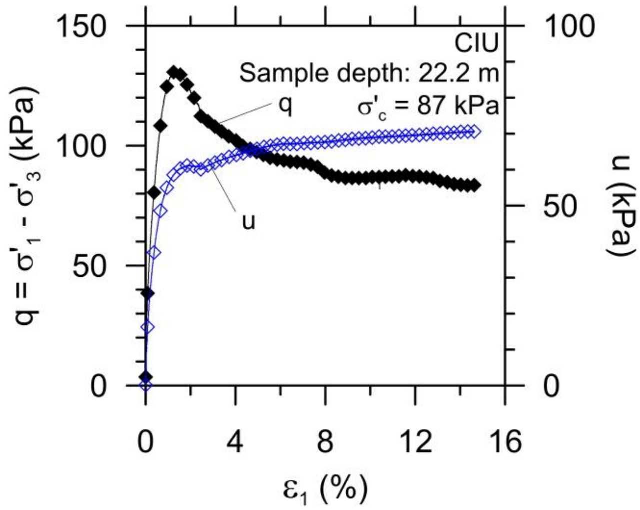

Figure 11 : Results of a triaxial undrained compression tests consolidated under an effective stress (σ'_c) of 87 kPa on a sample taken at a depth of 22.2 m from the borehole at location 32092.

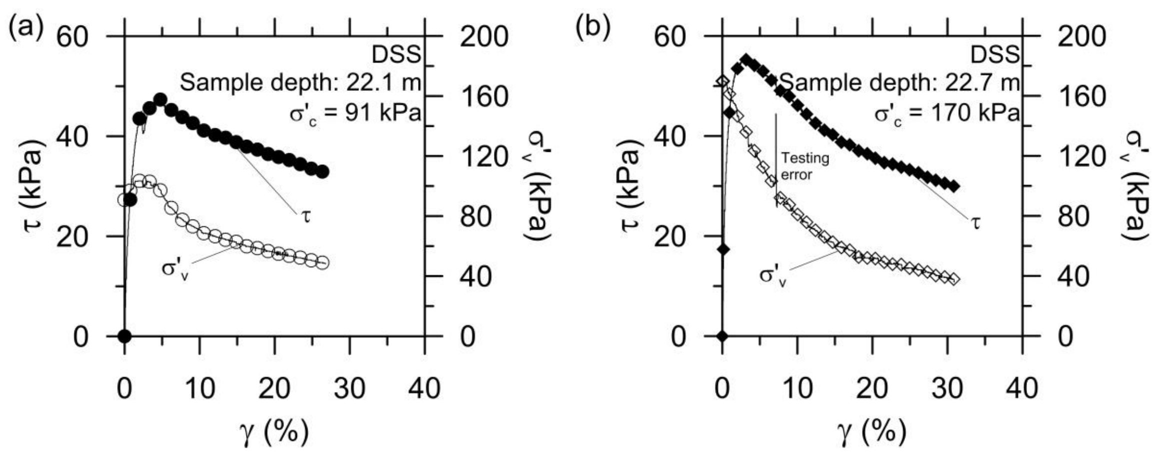

Figure 12 : Results of constant volume DSS tests (a) consolidated under an effective stress of 90 kPa on a sample taken at a depth of 22.1 m and (b) consolidated under an effective stress of 170 kPa on a sample taken at a depth of 22.7 m, both at location 32092.

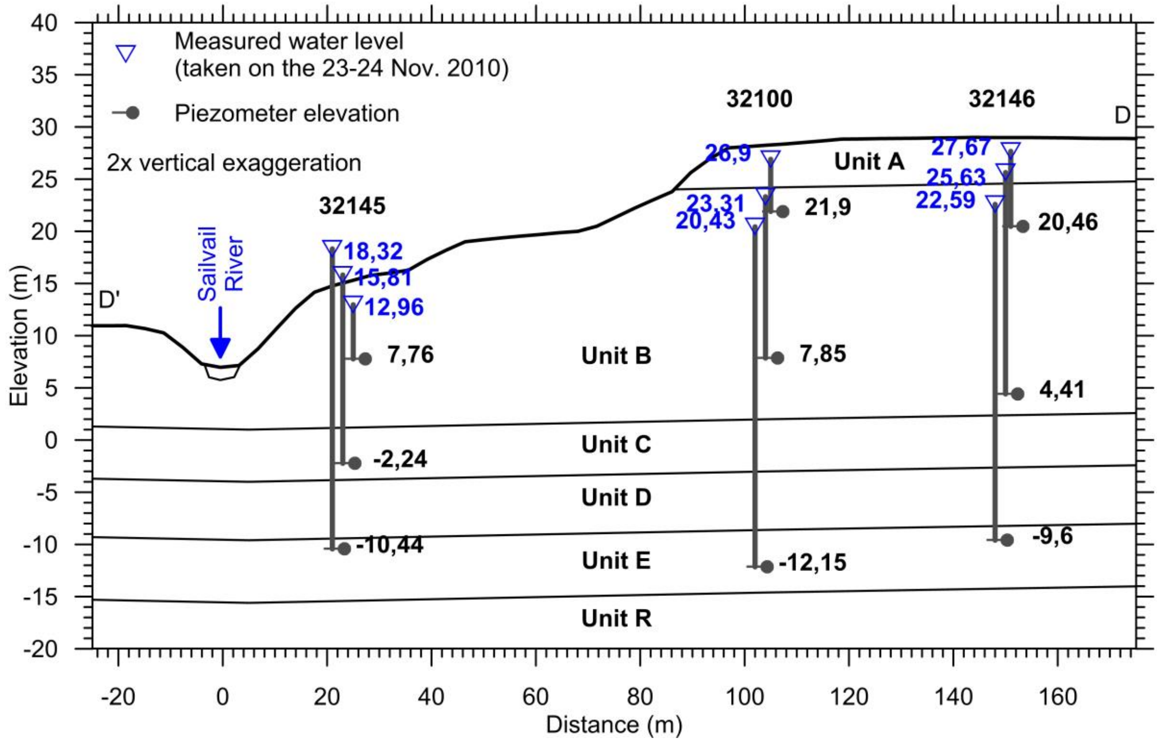

Figure 13 : Cross-section D-D', view toward the north, piezometers at location 32145, 32100 and 32146 (see Figure 3 for locations, modified from Locat et al. 2012a).

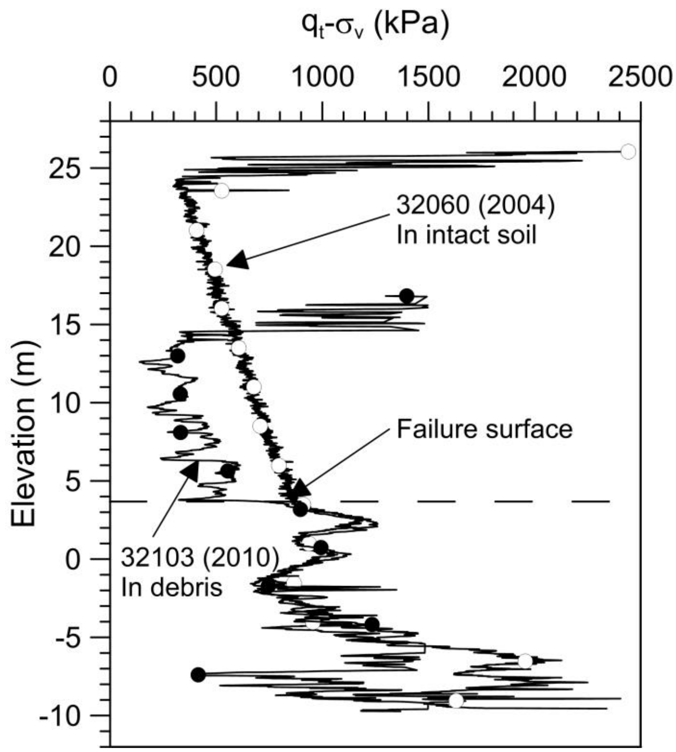

Figure 14 : Failure surface identified by CPTU (see Figure 3 for location of CPTUs.

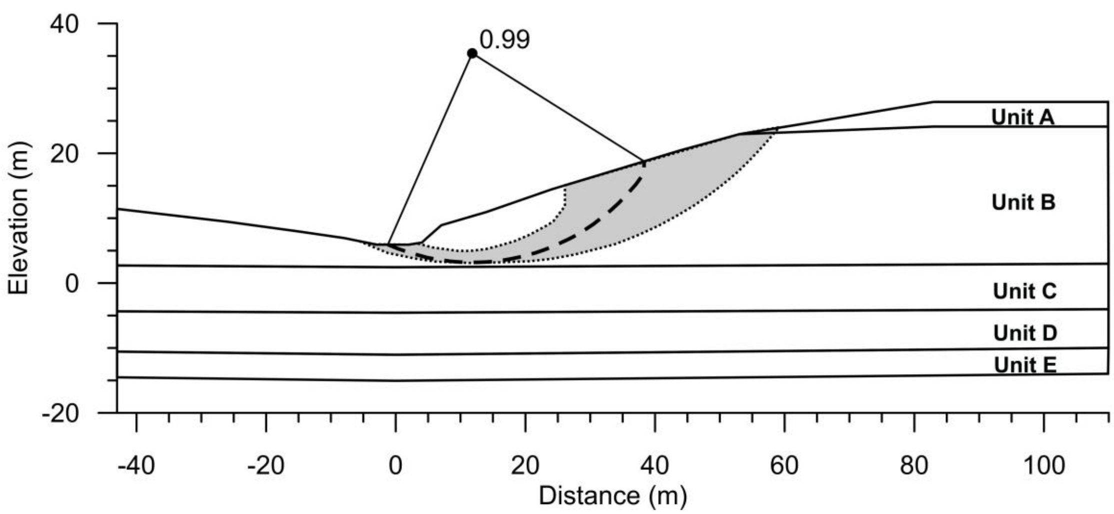

Figure 15 : Result of the drained stability analysis showing the critical failure surface (dashed line) and grey zone locating failure surfaces giving a safety factor lower than 1.05.

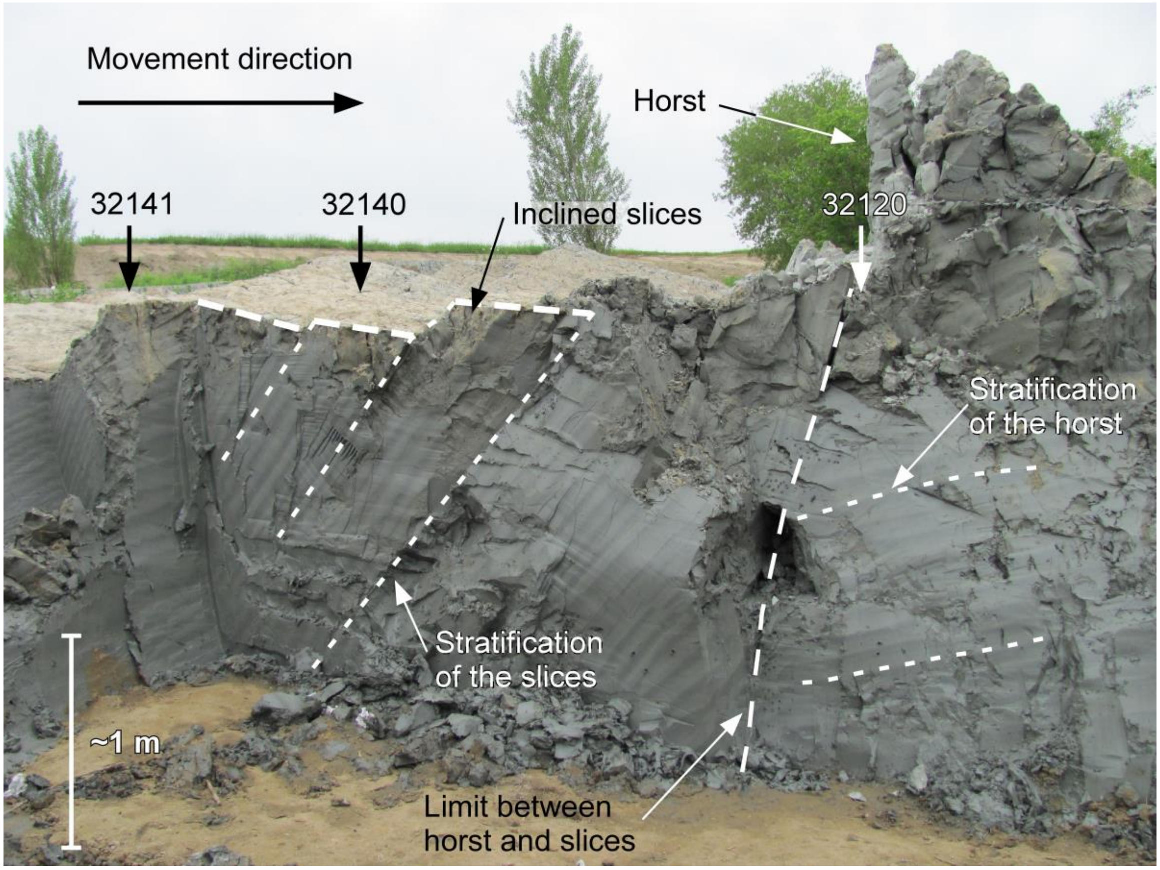

Figure 16 : View toward the south-west of the trench 32152 and approximate location of sites 32120, 32140 and 32141 (see Figures 3 and 9 for location). The picture was taken on June 16th 2010, about a month after the landslide (modified from Locat et al. 2012a).

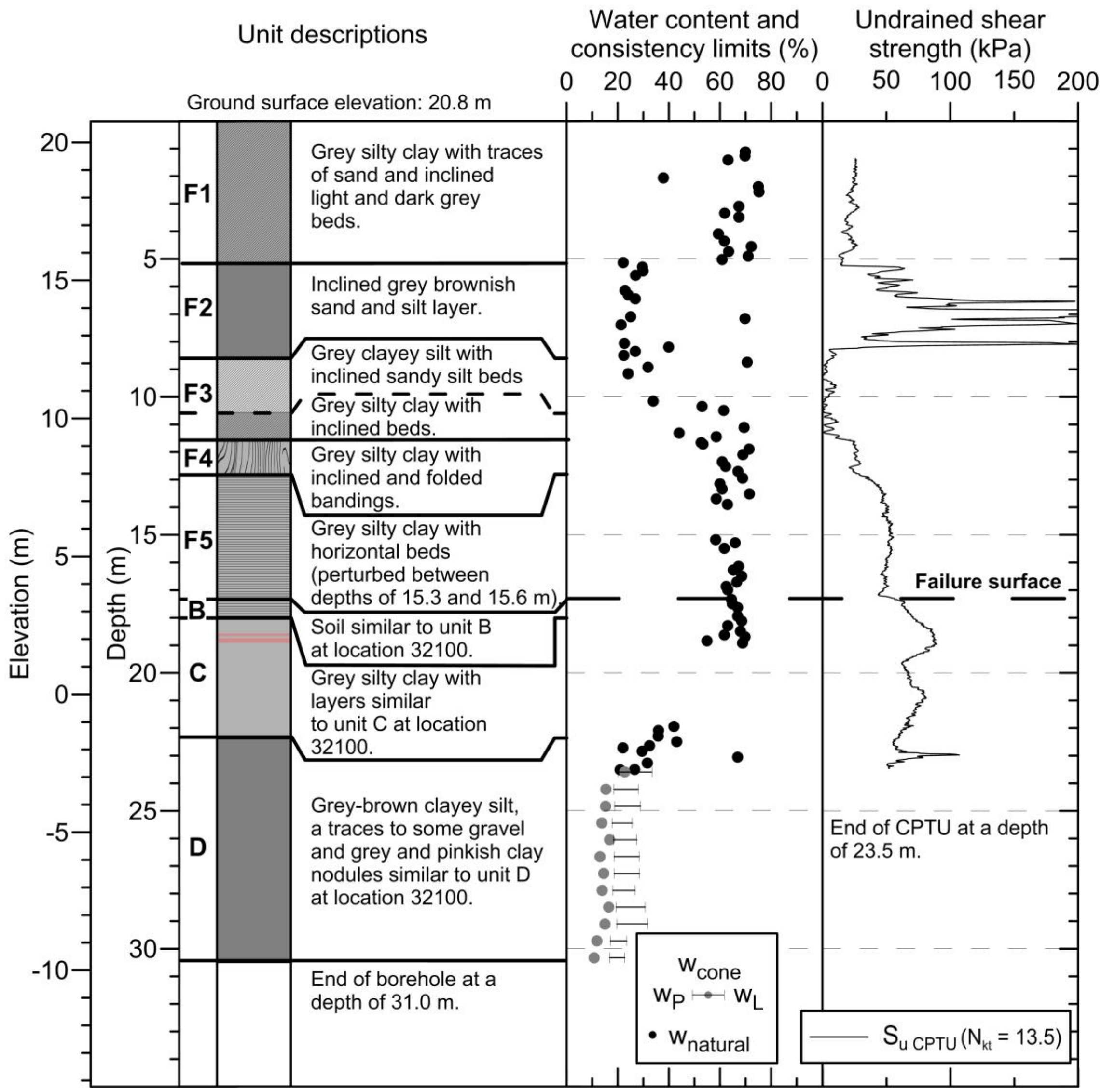

Figure 17 : Geotechnical profile at location 32140 in the debris (see Figure 3 for location).

936 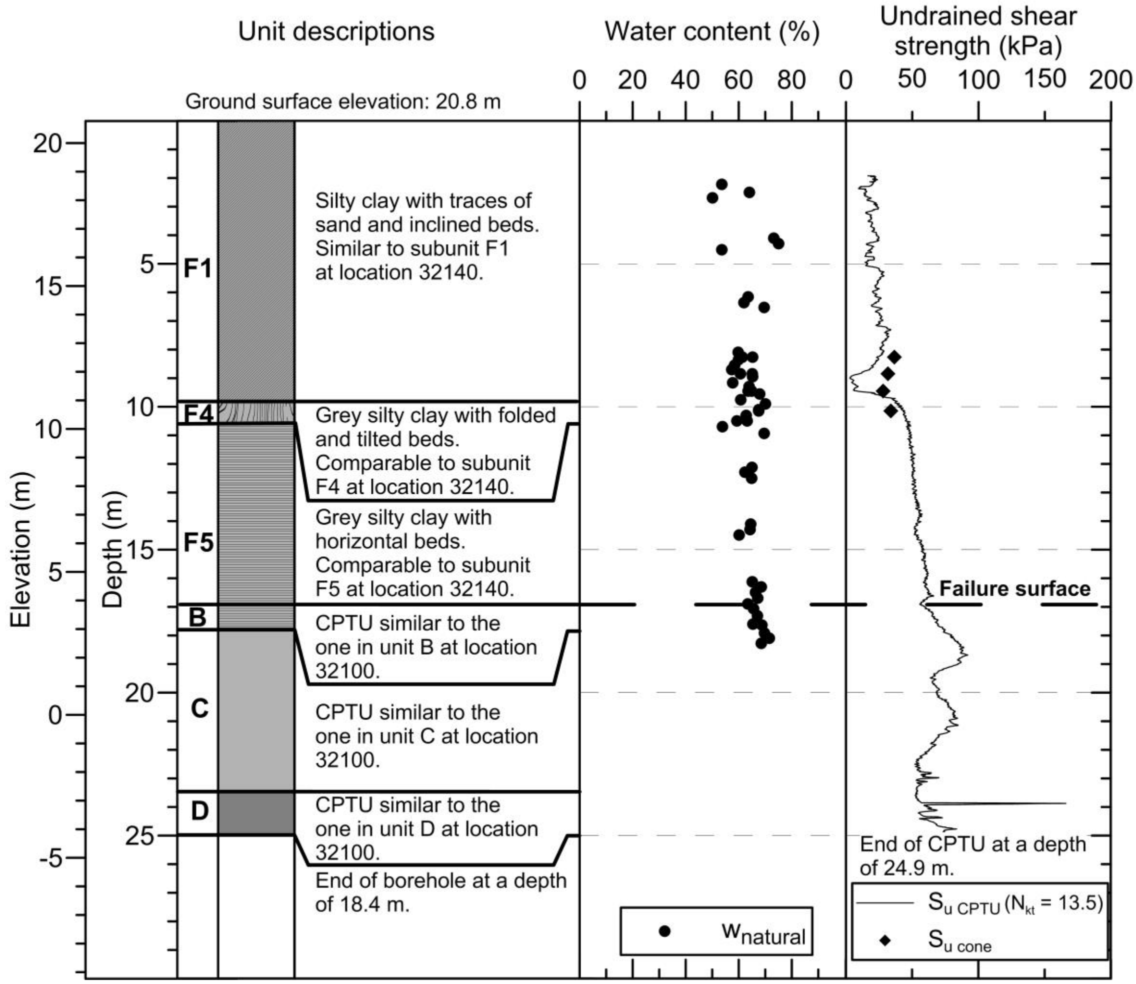

937 Figure 18 : Geotechnical profile at location 32141 in the debris (see Figure 3 for location).

938 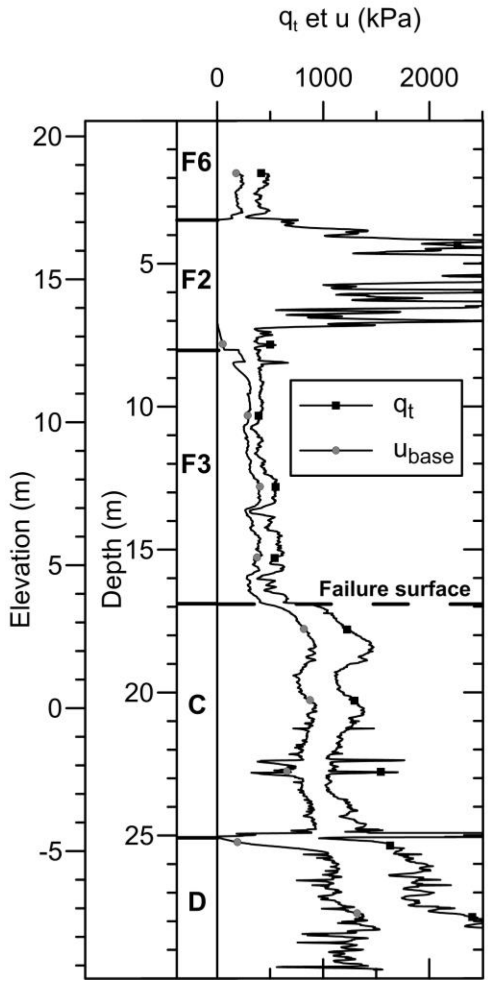

939 Figure 19 : CPTU profile at location 32120 in the debris and corresponding units as
940 described on Figures 17 and 18 (see Figure 3 for location).

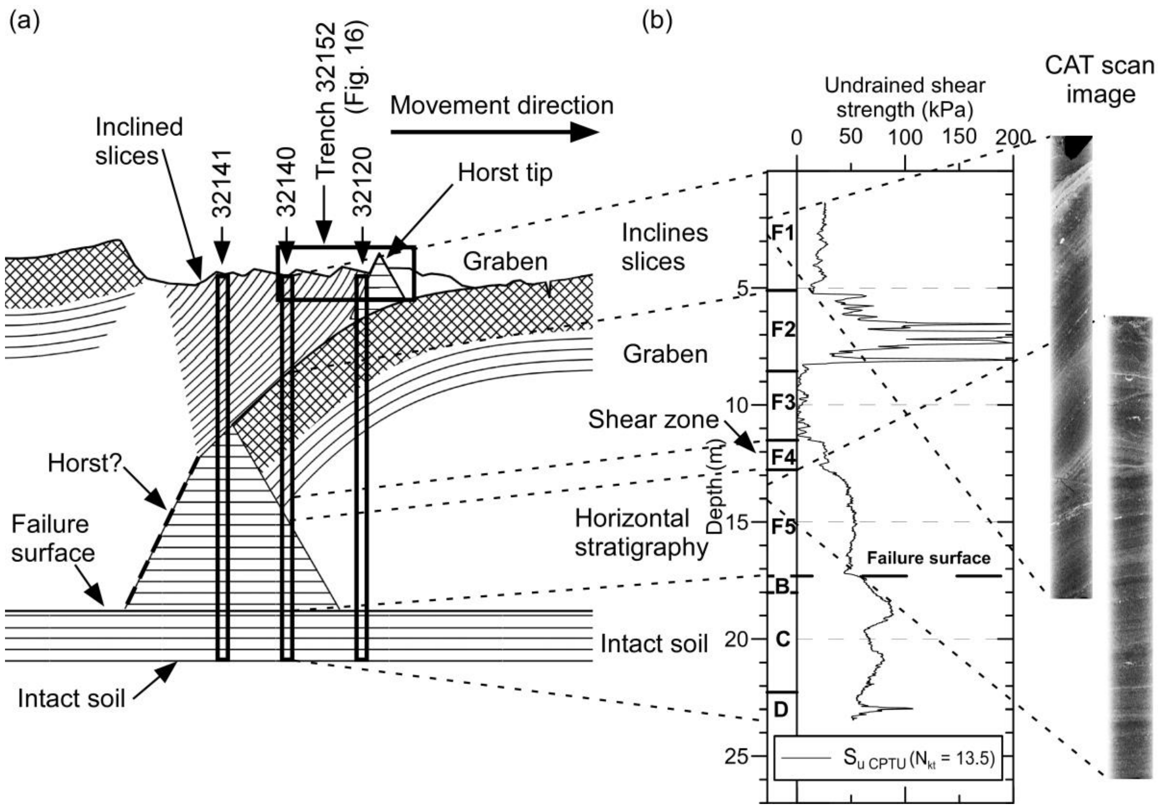

Figure 20 : a) Approximate interpretation of the stratigraphy near trench 32152 (Figures 9 and 16), view toward the south-west, including location of soundings and b) example of CPTU and CAT scan results at location 32140 (see Figures 3 and 9 for location, modified from Locat et al. 2012a).

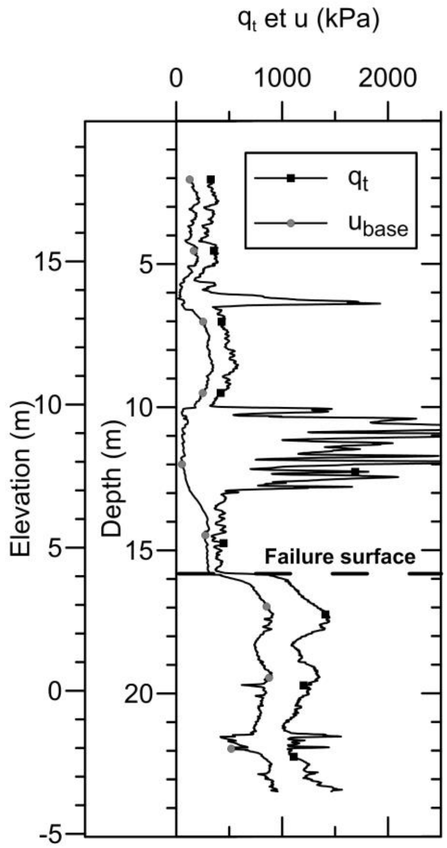

Figure 21: CPTU profile at location 32118 in the debris showing the sandy crust, introduced on figure 10, buried at a depth 10 m under a layer of silty clay (see Figure 3 for location).

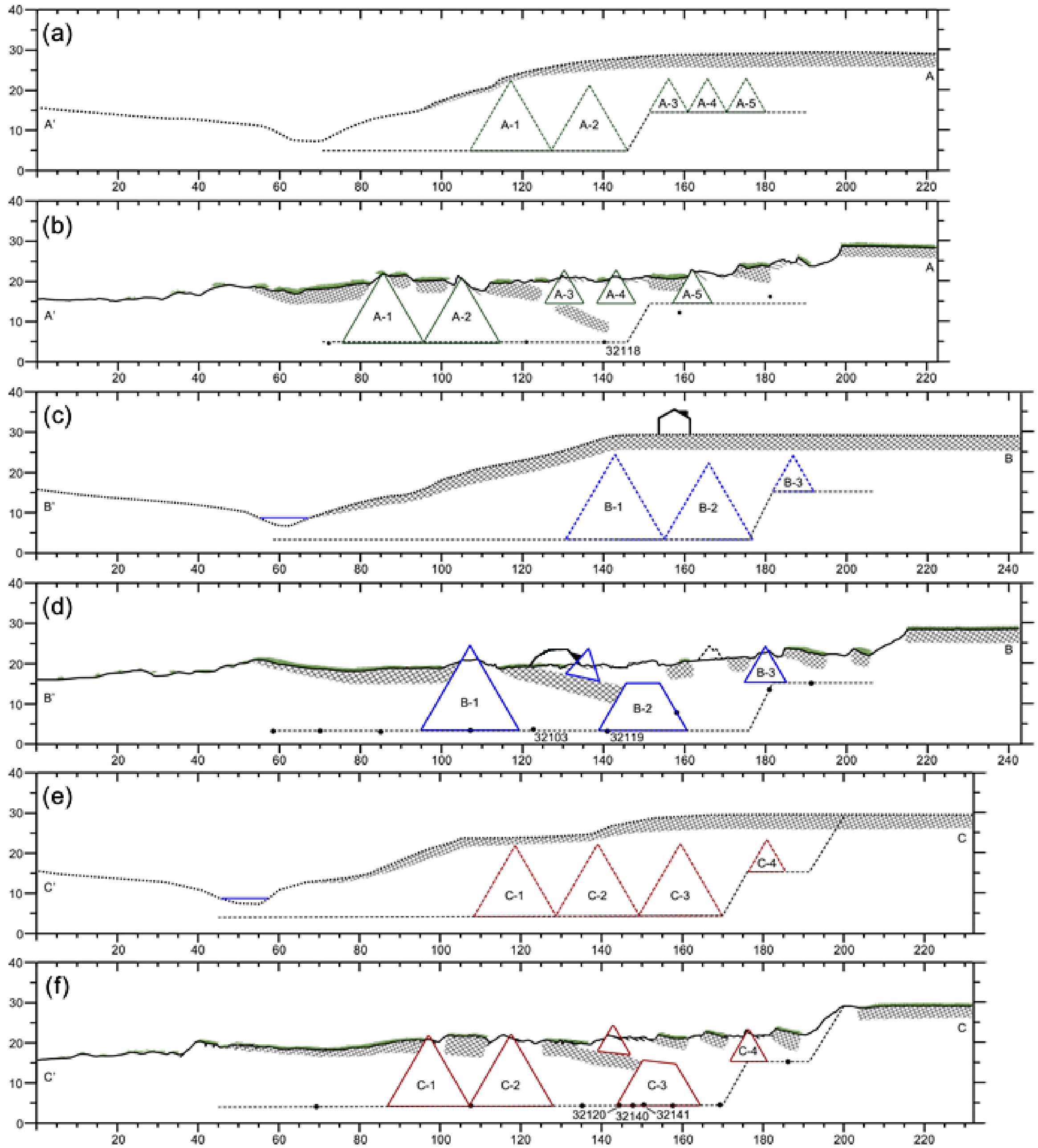

Figure 22: Drawing showing suggested position of each horst and graben before (a, c and e) and after (b, d and f) the landslides for cross-sections A-A’, B-B’ and C-C’.